Ph.D. Dissertation of Natural Science

Neural correlates of visual scene memory- dependent behavior in the subiculum

시각장면기억 과제에서 해마이행부의 역할

February 2019

Graduate School of Natural Sciences
Seoul National University
Brain and Cognitive Sciences Major

Su-Min Lee

Neural correlates of visual scene memory-dependent behavior in the subiculum

Inah Lee
Submitting a Ph.D. Dissertation of Natural Sciences

February 2019

Graduate School of Natural Sciences
Seoul National University
Brain and Cognitive Sciences Major

Su-Min Lee

Confirming the Ph.D. Dissertation written by
Su-Min Lee
February 2019

Chair	이 석 호	(Seal)
Vice Chair	이 인 아	(Seal)
Examiner	곽 지 현	(Seal)
Examiner	이 준 열	(Seal)
Examiner	최 지 현	(Seal)

Abstract

The hippocampal formation, the hippocampus and subiculum, is important for spatial memory as well as episodic memory both of which visual scene information plays critical roles. Our laboratory has reported that hippocampal damage induces impairment in a visual scene memory task. In the same task, neurons in the hippocampus show scene-dependent rate-remapping. Based on our prior results, damage in the subiculum also impairs performance in the task. However, the neural correlates of visual scene information processing in the subiculum are largely unknown. When analyzing neural spiking data from the subiculum using event rate map-based procedures, the neural activity in the subiculum was modulated by the scene stimulus. However, the firing rate-based analytical protocol might not be sufficient to capture the subicular neuronal functions because of the broad and continuous firing patterns of the subicular fields. To resolve such analytical issues, in the present thesis, subicular firing fields were spatially defined by their relationships with the local theta rhythm (i.e., theta phase precession). This phase-based method finds latent firing fields in the subiculum more efficiently compared to the conventional rate-based method. It is also confirmed that the subiculum represents scene information by rate-remapping as similarly as the hippocampus does. Putting together, visual scene information is robustly represented in both the hippocampus and subiculum when analyzed by different methods. However, more heterogeneous classes of firing fields are

found in the subiculum than in its upstream region, CA1, in terms of their hypothesized functions as to representing specific location versus more chunked epochs of the task. Such critical differences may arise in the process of transforming the location-bound code of the hippocampus to more behavioral response-oriented code in its downstream structures including the subiculum.

Keyword : subiculum, hippocampus, place cell, scene memory, rate-remapping, theta phase precession

Student Number : 2013-22456

Table of Contents

Abstract i

List of Figures iv

Background 1

EXPERIMENT 1. Representation of Visual Scene in the CA1 and Subiculum based on Firing Rates 9

Introduction 10

Materials and Methods 12

Results 23

Discussion 40

EXPERIMENT 2. Representation of Visual Scene in the CA1 and Subiculum after the Theta Phase-based Parcellation of Spiking Activities into Place Fields 42

Introduction 43

Methods 45

Results 49

Discussion 67

General Discussion 68

Bibliography 77

국문 초록 87

List of Figures

Figure 1. Inactivation of the subiculum (SUB) impaired the performance in visual scene memory task. 11

Figure 2. Behavioral paradigm and experimental schedule. 17

Figure 3. Behavioral performance in VSM task. 24

Figure 4. Simultaneous recording of single units from the CA1 and subiculum. 26

Figure 5. Basic firing properties of single units in the CA1 and subiculum. 28

Figure 6. Basic firing properties of single units in the CA1 and subiculum. 30

Figure 7. Types of firing fields in the CA1 and subiculum. 34

Figure 8. Task-dependent rate remapping in the CA1 and subiculum. 36

Figure 9. Comparison of rate remapping between the CA1 and subiculum. 39

Figure 10. Theta phase precession clearly observed in the subiculum. 50

Figure 11. DBSCAN algorithm used for detection of place fields. 54

Figure 12. Validity of clustering tested by quality measurements. 57

Figure 13. Examples of TP-based place fields in the CA1. 59

Figure 14. Examples of TP-based place fields in the subiculum. 60

Figure 15. Changes in firing properties between FR- and TP-based firing fields. 62

Figure 16. Differences in properties of theta phase precession between the CA1 and subiculum. 64

Figure 17. Task-dependent rate-remapping in the TP-based firing fields. 66

Figure 18. Schematic firing patterns of the neural populations in the subiculum, but not in the CA1. 71

Figure 19. Illustration of the differential coding schemes between the hippocampus and subiculum. 72

Background

1. Significance of hippocampus in visual scene-dependent memory

Hippocampus is known as the hub area responsible for episodic memory and spatial memory. In the study of human patient Henry Gustav Molaison, surgical resection of medial temporal lobe including the hippocampus induced moderate retrograde amnesia and severe anterograde amnesia, which proposed a pivotal role of the hippocampal formation for episodic memory (Scoville and Milner, 1957). In experiments involving animals, it was found that hippocampal neurons are highly correlated with animal's location (O'Keefe and Dostrovsky, 1971), which are thought to be the neural basis of the cognitive map (O'Keefe and Nadel, 1978). Prior studies have discovered that these hippocampal place cells play key roles in other mnemonic functions as well (Hasselmo and Schnell, 1994; Treves and Rolls, 1994; Eichenbaum, 2000; Lee et al., 2004).

In line with the idea, it was proposed that the hippocampus also supplies the ability to process scene-dependent memory, a crucial ingredient for various cognitive functions including episodic memory, spatial navigation, and imagining future plans (Maguire and Mullally, 2013). This idea is supported by prior studies reporting that bilateral hippocampal damages induced deficits in scene information processing in human (Hassabis et al., 2007; Mullally et al., 2012) as well as nonhuman primate (Gaffan and Harrison, 1989; Gaffan, 1994). Rodent studies also found that the hippocampus is involved in

acquisition and retrieval of episodic memory based on contextual environment (Kim and Fanselow, 1992) and that firing activities of hippocampal neurons were modulated by distinctive changes in external visual cues (Muller and Kubie, 1987; Markus et al., 1995; Anderson and Jeffery, 2003; Leutgeb et al., 2005; Colgin et al., 2008). Recent studies in our laboratory further provide the evidence that the hippocampus is critical for processing scene information and making an associated behavioral response choice. The inactivation of bilateral hippocampus in rats impaired performance in scene-dependent spatial choice task (Kim et al., 2012a; Delcasso et al., 2014; Lee et al., 2014) and single unit recording in the same experimental paradigm revealed the firing rate modulation of place cells in hippocampal subfield Cornu Ammonis 1 (CA1) depending on scene stimulus presented to the subject (Delcasso et al., 2014).

2. Differences between the hippocampus and subiculum, the primary source of hippocampal efferents

Subiculum is a part of the hippocampal formation, located between the hippocampus and the entorhinal cortex. Although the subiculum anatomically sits at an important position that might be suitable to send hippocampal information to other cortical and subcortical areas, a number of literatures reported that anatomical and physiological characteristics of the subiculum are quite different from those of the hippocampus.

Unlike the five-layered appearance of the hippocampus, subiculum consists of three principle layers: a molecular layer, continuous with stratum radiatum and stratum lacunosum-moleculare of the CA1; an enlarged pyramidal cell layer containing the soma of principal neurons; and a polymorphic layer continuous with the stratum oriens of the CA1. The principle cell type of the subiculum is pyramidal cell, the same as CA1, but the packing of subicular pyramidal cells is much looser than CA1.

The subiculum is primarily innervated by the CA1 and the entorhinal cortex in topographical manner along the proximodistal axis (Steward, 1976; Amaral et al., 1991; Witter, 2006). In specific, proximal subiculum has afferent projections from distal CA1 and lateral part of entorhinal cortex, whereas distal subiculum from proximal CA1 and medial part of entorhinal cortex. The topographic organization of the projections from the entorhinal cortex to the subiculum is in the opposite direction to the CA1. Both regions

receive entorhinal inputs from the superficial layer, but send outputs to deep layer. The subiculum has been reported to have reciprocal connections with perirhinal cortex and postrhinal cortex to which the CA1 is also connected, while the afferents from the postrhinal cortex and efferents from both regions are denser in the subiculum (Naber et al., 2001; Agster and Burwell, 2013). In addition, the areas connected to both the CA1 and subiculum include presubiculum, parasubiculum, retrosplenial cortex (Naber and Witter, 1998) and nucleus reuniens (Wouterlood et al., 1990).

However, based on the technological advances, recent studies have discovered unique connections of the subiculum. The basal amygdalar input, lacking in dorsal CA1, directs to the proximal part of the dorsal subiculum (Cembrowski et al., 2018), indicating that the subiculum receives a much various type of information. The visual cortex also gives a direct projection to the subiculum (Sun et al., 2019), which is thought to provide additional information about the external environment. In the other hand, the proximal part of the dorsal subiculum directly innervates medial prefrontal cortex (Cembrowski et al., 2018) and nucleus accumbens (Naber and Witter, 1998), to which the ventral part is primarily connected in the hippocampal formation. Moreover, subicular cells back-projecting to the CA1 have been reported (Sun et al., 2014; Sun et al., 2019), suggesting the possibility of subicular functions beyond the unidirectional information flow in the hippocampal formation.

Differences between the CA1 and subiculum also featured in electrophysiological findings. When recording the single units from

freely moving animals, the spatial code of the subiculum differed from that of the hippocampus. The hippocampal place cells generally have a single firing field at a narrow and focal place, whereas the subicular neurons exhibit poor spatial tuning with a broad firing field (Barnes et al., 1990; Sharp and Green, 1994) or multiple firing fields (Kim et al., 2012b). Also, some studies demonstrated that firing activities in the subiculum were relatively less sensitive to the changes in geometry or visual cues in the external environment (Sharp, 1997, 2006; Brotons-Mas et al., 2017). In addition, some neural correlates of spatial navigation in the subiculum have been reported, including boundary-vector cells (Lever et al., 2009) and axis-tuned cells (Olson et al., 2017). A few subicular cells exhibited strong directional selectivity in their firing fields (Sharp and Green, 1994) or grid-like firing patterns (Brotons-Mas et al., 2017). Other studies reported some different firing patterns between the hippocampus and subiculum in a working memory task (Hampson et al., 2000; Deadwyler and Hampson, 2004).

Beyond the inter-regional differences, recent research has focused on the functional differences between cell types within the subiculum. According to the studies with *in-vitro* recordings, the subicular pyramidal cells are classified into at least two types based on their firing responses to intracellularly injected depolarizing current: intrinsic bursting cells or regular spiking cells (Behr et al., 1996; Harris et al., 2001). These subicular cell types differ in synaptic plasticity (Fidzinski et al., 2008; Behr et al., 2009), form different recurrent connections (Bohm et al., 2015), and are

distributed differently along the anatomical axis (Jarsky et al., 2008; Cembrowski et al., 2018). Anatomical subdivisions of the subiculum along the proximodistal axis also exhibit differences in the gene expression, afferent and efferent connections to the cortical and subcortical areas, and the firing properties (Kim et al., 2012b; Kim and Spruston, 2012; Cembrowski et al., 2018). *In-vivo* electrophysiological studies also divided subicular cells into bursting and non-bursting groups to identify differences in spatiotemporal codes (Sharp and Green, 1994; Anderson and O'Mara, 2003), or sparsely and dominantly bursting groups with differences in spatial firing patterns (Simonnet and Brecht, 2019).

Based on the unique connections and physiological characteristics that are different from CA1, the hypothesis about subicular function has been raised to make conjunctive representation by integrating information gathered from various brain areas (Matsumoto et al., 2019). Combining with the heterogeneity of neural activities within the subiculum, it can be argued that subicular subpopulations work in a complementary manner by reorganizing information in different ways and distributing it to different information pathways.

3. Importance of understanding subicular neural correlates in scene-dependent memory processing

Despite the anatomical and physiological investigation of the subiculum in literature, there is still a lack of understanding of the functional roles of the subiculum in hippocampal-dependent memory. The search for the subicular mnemonic function has been conducted in spatial working memory tasks (Hampson and Deadwyler, 2003; Potvin et al., 2007; Potvin et al., 2010), spatial navigation (Cembrowski et al., 2018), and contextual fear conditioning (Roy et al., 2017), but most of these experiments just examined behavioral changes induced by temporary inhibition of subicular neurons with physiological evidence missing. To date, subicular neural correlates have been interpreted mainly in terms of spatial factors based on simple behavioral protocols such as foraging and shuttling. In a few prior studies, non-spatial activities of the subicular neurons were examined using objects (Chang and Huerta, 2012) and rewards (Martin and Ono, 2000; Gauthier and Tank, 2018). However, none of those experimental paradigms was likely to recruit either the hippocampus or subiculum. Considering that CA1 place-field activity is also frequently modulated by non-spatial factors, a coherent theoretical framework is required to understand the functional significance of the subicular firing patterns in relation to those in the CA1. Therefore, it is necessary to design a behavioral task demanding associative memory between spatial and non-spatial components, dependent on both the hippocampus and subiculum.

Several previous studies have suggested that the subiculum is important for scene memory (Potvin et al., 2009; Roy et al., 2017). Compared to those studies, the results of our recent study provide the most direct evidence for the significance of the subiculum in scene memory, showing that the malfunction of bilateral subiculum impaired performance in a visual scene-dependent spatial choice task (unpublished). Although the hippocampal cells seem to be specialized in representing highly localized areas, one may be surprised if those individual place fields are associated with different scenes because an allocentric visual scene may remain constant even if an agent moves across individual locations. In other words, scenes rarely change unless the animal moves a significant distance in space. Therefore, it begs the question whether the detailed spatial representation of the hippocampal place cells is proper for scene-dependent decision making. On the other hand, the place cells in the subiculum exhibit broadly-tuned fields and distinctive firing patterns related to movement. Considering all these, it would be reasonable to claim that the neural mechanism of scene-dependent behavioral decision may be more related to the subicular firing patterns instead of those in the hippocampus. In the current thesis, I will conduct several experiments and analyses to test this hypothesis.

EXPERIMENT 1. Representation of Visual Scene in the CA1 and Subiculum based on Firing Rates

Introduction

It is well established that the hippocampal formation is important for visual scene memory. In our previous studies, behavioral impairment was observed in the task requiring spatial response associated with visual scenes, when the dorsal hippocampus was injected with $GABA_A$ agonist muscimol to inactivate neural activities (Kim et al., 2012a; Delcasso et al., 2014). In addition, task performance decreased in the same paradigm even when the subiculum, which is thought to deliver hippocampal scene information to cortical areas as the major output structure of hippocampus, was inactivated (**Figure 1**). According to the previous literatures, rats without the subiculum exhibit behavioral deficiencies in distinguishing visual scenes with a high degree of overlap (Potvin et al., 2009), and mice with CA1−SUB projection selectively disabled by optogenetic methods failed to learn a contextual fear conditioning task (Roy et al., 2017). Combining the evidences, it is suggested that subiculum is also involved in processing scene information and performing its associated responses.

In a visual scene memory task, the neural activity within the place field in CA1 is modulated by visual scenes presented to the rat (Delcasso et al., 2014). However, it has not been investigated whether subicular cells have neurophysiological correlate for the scene as well. Therefore, I tested whether the subicular cells represented scene information through the firing rate modulation

within the place fields as has been reported with the hippocampal place cells by recording the single unit activities of the subiculum simultaneously with the CA1 in the visual scene memory task.

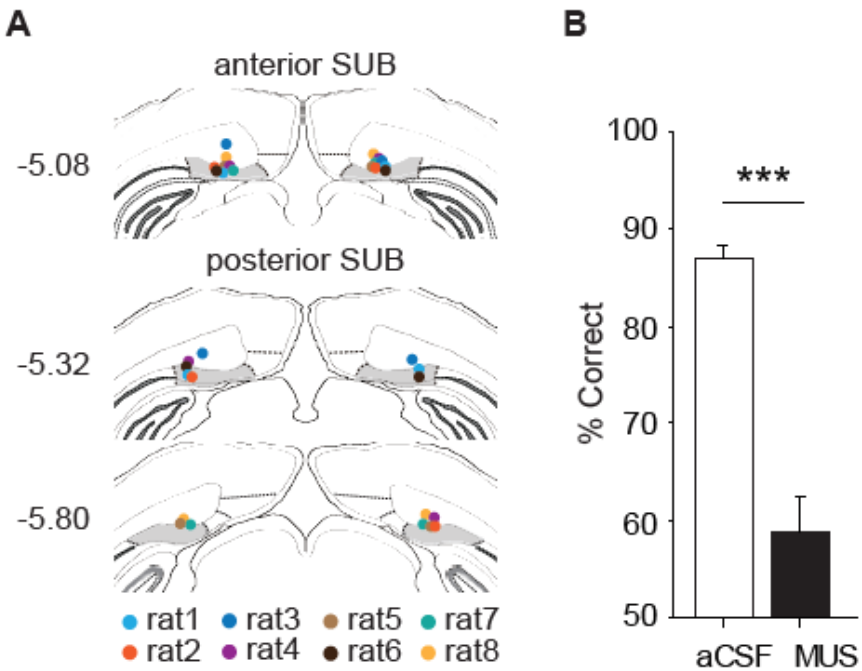

Figure 1. Inactivation of the subiculum (SUB) impaired the performance in visual scene memory task. (A) Cannula-tip positions in the SUB (color-coded by rat). Numbers on the left indicate relative distance (mm) from bregma. SUB is marked with gray background. (B) Significant impairment in performance following muscimol (MUS) injections into the SUB compared with vehicle (aCSF) injections. Mean ± S.E.M. ***P < 0.001, one-sample t-test. (unpublished data)

Materials and Methods

Subjects

Seven male Long-Evans rats weighing 300-400g were used. All animals were housed individually under a 12 h light/dark cycle. For behavioral experiments, food was restricted to maintain body weight at 85% of the free-feeding weight with free access to water. All protocols are in compliance with the Institutional Animal Care and Use Committee of Seoul National University.

Behavioral apparatus

An elevated T-shaped track (47×8 cm stem for 1 rat and 73×8 cm stem for others with two 38×8 cm arms) containing a food well (2.5 cm diameter, 0.8 cm deep) at the end of each arm was used for the behavioral experiment (Figure 2A). A guillotine door-operated start box (16×22.5×31.5 cm) was attached at the bottom of the stem. Three 17-inch LCD monitors were positioned as an array surrounding the upper portion of the track to provide visual scene stimuli. Four pairs of optic fiber sensors (Autonics) were installed along the stem at different points (1, 27, 47 and 67 cm from the entrance of the start box) to detect the animal's position and to control the onset of the scene stimuli. Additional optical distance sensors were installed inside the food wells to record the moment the rat obtained the reward. Sensor activities were transmitted to a data-acquisition system (Digital Lynx XS, Neuralynx) as a

transistor–transistor logic (TTL) signal. We used custom–written software created in MATLAB (MathWorks) and Psychtoolbox to control scene stimuli. The apparatus was located in a soundproof room, and white noise was played by two loudspeakers (80 dB) during behavioral sessions to mask unwanted environmental noise. The apparatus was surrounded by black curtains and dimly lit by a ceiling lamp. A digital camera attached to the ceiling recorded both positions and directions of the animal's head at a sampling rate of 30 Hz.

Visual scene memory (VSM) task

In the VSM task, the experimenter started a trial by manually opening the door of the start box. This opening was detected by the optical sensor, immediately triggering the display of the visual scenes on the monitors. The rat ran along the track toward the end of the stem to choose either the left or right arm in association with the visual scene (Figure 2A). The food well in the arm that was correctly associated with the scene contained a quarter piece of cereal reward (Froot Loops, Kellogg's), and the rat obtained the reward by displacing a black acrylic disk covering the food well. If the rat made an incorrect choice, no reward was provided. The rat was gently guided back to the start box immediately after either correct or incorrect choice was made. An intertrial interval (10s) was given after a correct trial; a longer intertrial interval (20s) was given after an incorrect trial. The experimenter placed a reward in one of the food wells for the next trial (following the predetermined baiting sequence) during the

intertrial interval. The rat was confined in the start box during the intertrial interval, and the high walls (31.5 cm) and background white noise (80 dB) in the room made it difficult for the rat to discern the next trial's baited food-well location from the start box.

Four grayscale visual patterns (zebra stripes, pebbles, bamboo, snow-covered mountains) were used as scene stimuli. The visual scenes were equalized for luminance (set at an average intensity value = 103 in Adobe Photoshop). For all trials, zebra stripes and bamboo patterns were associated with the food well in the left arm, and pebbles and mountain patterns were associated with the food well in the right arm. Rats were initially trained to criterion with a pair of visual scenes (≥75% correct choices for each scene for 2 consecutive days) and then were trained with the second pair of scenes. The training order of different scene pairs was counterbalanced among the rats. Forty trials were conducted in a presurgical training session. The presentation sequence of scene stimuli across trials in a given session was pseudorandomized with the following constraints: (1) each scene was presented equally in every 20 trials, and (2) the same food well was not used for rewards in four consecutive trials. Once rats learned both pairs of scenes according to criterion, a hyperdrive was implanted (Figure 2B).

Hyperdrive implantation

After behavioral training, a microdrive array (hyperdrive) composed of 24 tetrodes and 3 reference electrodes was implanted for recording single-unit spiking activities and local field potential from

the dorsal CA1 and subiculum. The final impedance of each wire was adjusted to 100–300 kΩ (measured in gold solution at 1 kHz with an impedance tester) 1 day before the hyperdrive was implanted. When the surgery was conducted, the rat was anesthetized with an intraperitoneal injection of sodium pentobarbital (Nembutal, 65 mg/kg), and its head was fixed in the stereotaxic frame (Kopf Instruments). And the anesthesia was maintained by isoflurane inhalation (0.5–2% isoflurane mixed with 100% oxygen) throughout the surgery. Before making an incision along the longitudinal midline of the scalp, the scalpel blade and the incision area was sprayed with benzocaine for local anesthesia. A burr hole was drilled on the skull surface of the right hemisphere to insert the bundle of the hyperdrive. The target coordinates for implantation was predetermined to allow the electrodes to cover a range from 3.48–6.6 mm posterior to bregma and from 1–3 mm lateral to the midline. Then, the hyperdrive was chronically affixed to the skull with nine anchoring skull screws and bone cement. After surgery, ibuprofen syrup was orally administered to control the animal's general pain and the rat was left in a veterinary intensive care unit in which temperature and humidity were strictly controlled.

Electrophysiological recording

After a week of recovery from surgery, rats were retrained (~160 trials per session using the same pairs of scenes used before surgery) until they showed stable performance (≥75% correct choices for each scene). Over the course of a number of days during this

retraining period, tetrodes were lowered daily by small increments to reach the target areas. For tetrode adjustments, each rat was placed on a pedestal in a custom-made booth outside the behavioral experiment room. Neural signals were transmitted through the headstage (HS-36, Neuralynx) and tether attached to the electrode interface board of the hyperdrive to the data-acquisition system. Neural signals were digitized at 32 kHz (filtered at 600-6000 Hz) and amplified 1000-10,000 times.

Once the main electrophysiological recording session began, all four scenes used during the training period were presented in an intermixed fashion within a session (~160 trials per session). During the behavioral task, neural signals were relayed through a slip-ring commutator to the data-acquisition system, and an array of green and red LEDs was attached to the headstage to monitor the animal's positions and head directions using a ceiling camera. The rats performed the main recording sessions for 3-4 days (Figure 2B).

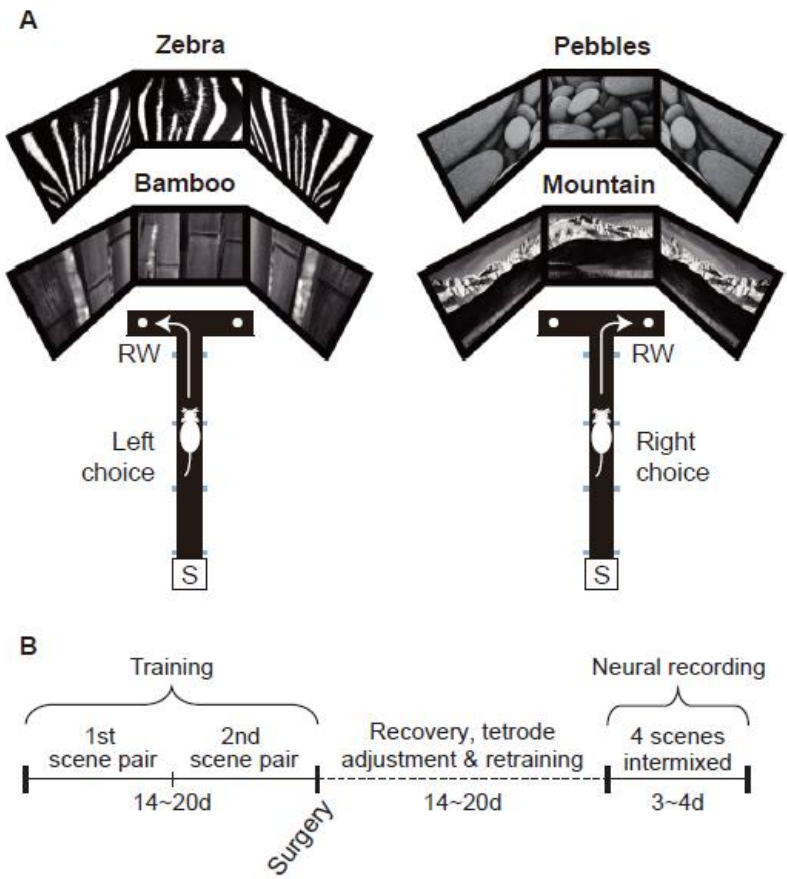

Figure 2. Behavioral paradigm and experimental schedule.(A) Illustration for VSM task. Scenes used as visual contexts. The rat chose an arm associated with the visual scene to obtain a piece of cereal in a food well. RW: reward, S: start box. (B) Overall experimental schedule of neural recording. After pre-surgical training of two pairs of scene stimuli respectively (Zebra and Pebbles for one pair, Bamboo and Mountain for another), 24-tetrode hyperdrive was implanted to target both CA1 and SUB. During re-training, tetrodes were adjusted. Once most tetrodes reached the target regions, neural activity was recorded while the rat performed behavioral task.

Histological verification of tetrode position

After the completion of all recording sessions, an electrolytic lesion was made via each tetrode (10 μA current for 10 s) to mark the tip position. After 24 h, the rat inhaled an overdose of CO2 and was perfused transcardially, first with PBS and then with a 4% v/v formaldehyde solution. The brain was extracted and soaked in 4% v/v formaldehyde–30% sucrose solution at 4° C until it sank to the bottom of the container. After postfixation procedures, the brain was gelatin–coated and soaked in 4% v/v formaldehyde–30% sucrose solution. The brain was sectioned at 30–40 μm using a freezing microtome (HM 430; ThermoFisher Scientific), after which sections were mounted and stained with thionin. Photomicrographs of brain tissues were taken using a digital camera (Eclipse 80i, Nikon) attached to a microscope, and were reconstructed three–dimensionally to match the configuration of the tetrodes from the initial bundle design. The exact locations of tetrodes were determined using the 3D reconstructed images and physiological depth profiles recorded at the time of data acquisition. To better present tetrode positions, we constructed a flat map of the dorsal CA1 and subiculum using Nissl–stained coronal sections and marked the tetrode positions in all rats in the flat map.

Construction of a flat map

A flat map was constructed using the coronal brain sections from all rats (**Figure 4A**). Nissl–stained sections were aligned to orient tetrode tracks vertically, and the length of the cell layer in the

subiculum and CA1 of each section was measured using an image processing software (ImageJ, NIH). Because the cell layer was curved along the transverse axis, multiple dots were first marked along the cell layer at narrow intervals, and the distance between the dots was calculated by summing their x and y positions. The marking procedures for dots started from the most distal end of the subiculum or CA1 and proceeded toward the proximal border. The lateral border of the flat map was based on the measured lengths of cell layers along the anterior–posterior axis. Because of individual differences in brain sizes and sectioning angles among rats, flat maps for all rats were proportionally adjusted by using the medial habenular nucleus and superior colliculus as references (Paxinos and Watson, 2009). After normalizing along the anterior–posterior axis, the length of the cell layer was finally determined by taking the median value of distances measured for all rats. The relative tetrode tip positions were then marked on the flat map.

Unit isolation

Single units recorded from the dorsal CA1 (n=364) and dorsal subiculum (n=320) were isolated manually using both commercial (SpikeSort3D, Neuralynx) and custom-written software (WinClust) using multiple waveform parameters, including peak and energy, as previously described (Lee and Kim, 2010; Delcasso et al., 2014). Neurons that did not satisfy the following set of criteria were excluded in further analysis: (1) average peak-to-valley amplitude of waveforms $\geq 75\,\mu V$ (79 units excluded), (2) proportion of spikes

within a 1 ms refractory period <1% of total spikes (5 units excluded), and (3) average firing rate during the outbound journey on the stem ≥1 Hz (174 units excluded). In addition, fast-spiking neurons (mean firing rate ≥10 Hz; width of the average waveform <325 μs) were excluded (n=55) from the analysis. Only those units that met the above criteria (n=129 in CA1, n=242 in subiculum) were used for final analysis. The reason behind the larger amount of neurons being filtered out in CA1 (n=133) than in the subiculum (n=41) was largely because many cells (approximately half of the isolated clusters) fired sparsely during the outbound journey in CA1, showing lower firing rates (<1 Hz), but that was not the case in the subiculum.

Spiking data analysis

Characterizing basic firing properties.

To measure the amount of spatial information conveyed by a unit, we constructed a linearized spatial rate map. Position data from behavioral sessions were scaled down (bin size = 4 cm2). Then, a raw spatial rate map was constructed by dividing the number of spikes by the duration of visit for each bin. The spatial rate maps were smoothed by moving average method for illustration purpose only. Spatial information was computed according to the following equation:

$$\text{Spatial information} = \sum_i p_i \frac{\lambda_i}{\lambda} \log_2 \frac{\lambda_i}{\lambda} \quad \text{(bits/spike)}$$

where i denotes bin, p_i is occupancy rate in the ith bin, λ_i is the mean firing rate in the ith bin, and λ is the overall mean firing rate.

The mean firing rate of a unit was obtained by averaging the firing rates in the raw rate map. Following the previous study (Kim et al., 2012b), a burst index was defined as the power of autocorrelation during 1−6 ms normalized by the power during 1−20 ms.

Construction of an event rate map.

We designated seven sequential task−relevant events as follows: trial start (opening of the door of the start box), three different time points detected by the optic sensors installed along the stem, spatial choice (turning to either the left or right arm), reaching the half point between the moment of spatial choice and reaching the arm end, and displacing the disc overlying the food well that contained reward. Timestamps for individual events were recorded by optic sensors, except for the choice event. Timestamps for the choice event were determined by detecting the spatial bin in which a significant difference between position traces associated with the left and right choice trials (two−sample t−test). The durations of individual events across trials were normalized and were split into three bins. Then, a raw event rate map (ERM) was constructed by dividing the number of spikes by the duration of occupancy for each bin. The raw ERM was smoothed using a moving average method to define field boundaries and for illustration purposes. However, all data analysis was conducted using raw ERMs.

Boundaries and categorization of event fields.

ERMs were categorized into three groups based on the number of

firing fields; single field (SF), multiple fields (MF) and event-unrelated fields. If the minimum firing rate of an ERM was larger than the half maximal firing rate, the rate map was classified as an event-unrelated field and the event-unrelated fields were excluded in the following analysis. The directions of change in firing rates across the events were measured by comparing the firing rates before and after the events to determine the boundaries of a field. That is, the firing rate of a bin was statistically compared with the firing rate in the next bin (using Wilcoxon rank-sum test) in an ERM to determine the direction of firing-rate changes (i.e., increase, decrease, and no change). The sequence of the changing direction in firing rate across the events made it possible to define local minima. Within the local minima, the bin with the maximal firing rate was defined as the peak of the field, and the boundaries were defined by detecting the bins in which the firing rates decreased to less than 40% of the peak firing rate. If there was no bin with the firing rate lower than the criteria, the local minimum became a field boundary. After defining the boundaries, cells were classified into two types: that is, a single field (SF) and multiple fields (MF) based on the number of the fields. A field with a ratio of the minimum to maximum firing rates exceeding 0.5 was not considered as a valid field. Field width was measured by counting the number of bins between the boundaries of a field. If there were more than one field in a rate map (i.e., MF), then each field was treated as independent fields.

Results

Rats successfully performed the VSM task relying on visual patterns

By the time when the recording of single units from the CA1 and SUB was conducted, all rats made correct choices in more than 85% of the trials for all scene stimuli, and performance for all scenes exceeded the criterion of 75% (P-values < 0.0001, one-sample t-test) (Figure 3).

It is possible that rats could solve the VSM task using only local features of the visual scenes. I tested this possibility using a separate group of rats (male Long-Evans, n = 10). Specifically, after being trained to criterion in the VSM task, rats were tested with masked scenes in some trials within a session. Rats were able to see the overall visual patterns through regularly spaced viewing holes in the masked scenes. Two masking patterns with different sizes of viewing holes (mask pattern 1 and 2) were used. In each session, one of the two pairs was chosen from mask pattern 1 and 2, and those individual masking patterns were pseudo-randomly presented in an intermixed fashion throughout the session with the original scene. Since a pair of masking patterns covered different portions of the original scene, focusing on fixed local features should be difficult in the masked trials. In this control experiment, the average performance levels of rats in the masked trials dropped from the performance level in unmasked trials (original vs. mask pattern 1, $Z = 2.7$, $P < 0.01$; original vs. mask pattern 2, $Z=2.66$, $P < 0.01$; mask pattern 1 vs. pattern 2, $Z = 1.44$,

P = 0.15; Wilcoxon signed-rank test), understandably as the scenes were not as clearly discernible in the masked trials as in unmasked conditions. However, it is important to note that performance in masked trials remained well above chance level (50%) (P-values < 0.01, Wilcoxon signed-rank test), suggesting that rats used the overall visual pattern in the scene as a cue instead of particular local features.

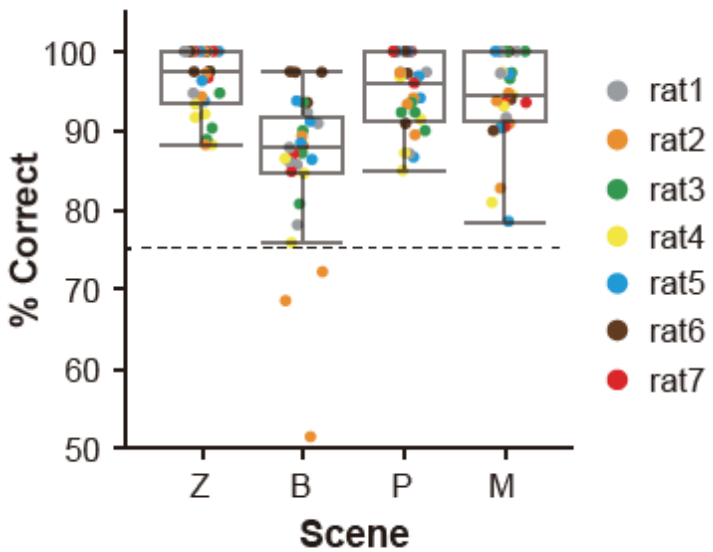

Figure 3. Behavioral performance in VSM task. Performance for each scene stimulus during recording sessions (color-coded for individual rats). Performance exceed criterion (dashed line, 75%) for all scenes.

Simultaneous recording of single units from the CA1 and subiculum

The locations of tetrode tips were reconstructed on a flat map (Figure 4A), using both histological results (Figure 4B) and physiological recording profiles. The recording locations were distributed approximately 3.5 to 6.6 mm posterior to bregma. The units that satisfied our unit-isolation criteria (n = 129 in CA1; n = 242 in subiculum) were found along the entire proximodistal axis in both CA1 and subiculum although more CA1 units were recorded in the proximal portion than in the distal part. There was a narrow zone at the border between the distal CA1 and the proximal subiculum where cell layers of both regions overlapped (SUB/CA1 in Figure 4A and 4B). The units recorded from this region were assigned to either CA1 or subiculum using multiple criteria, including (a) the baseline firing rate recorded in the start box in the absence of the scene stimulus (< 1 Hz in the CA1 and > 4 Hz in the subiculum), (b) the morphological characteristics of the cell layers in Nissl-stained sections, and (c) the depth-profiles for individual electrodes recorded during the tetrode-adjustment period.

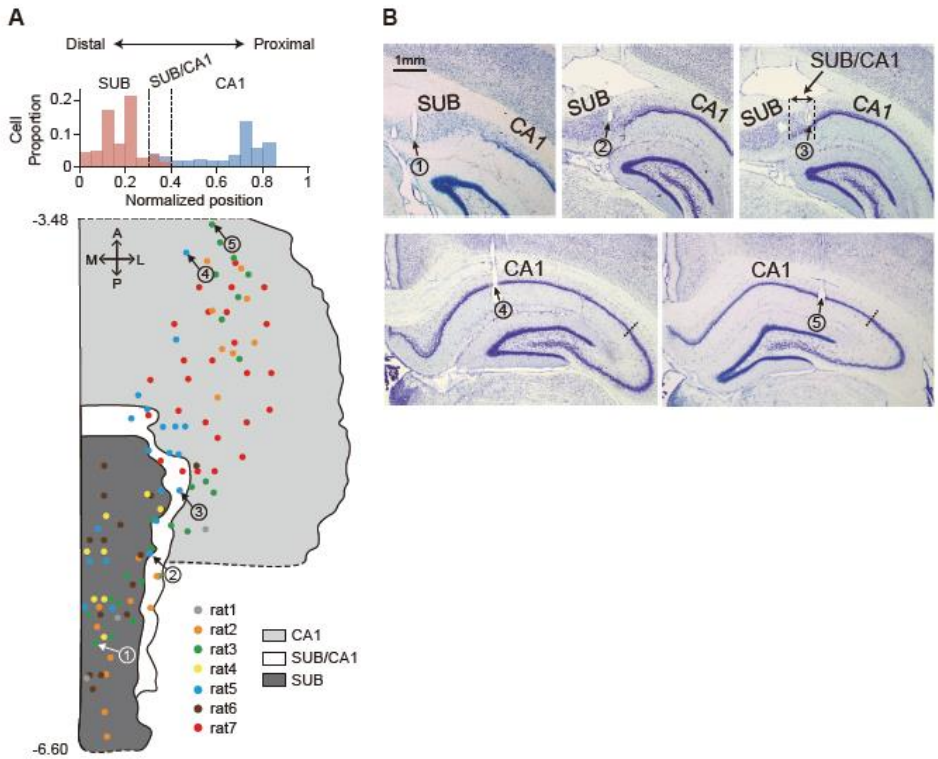

Figure 4. Simultaneous recording of single units from the CA1 and subiculum. (A) Proportional distribution of cells recorded in the CA1 (blue) and subiculum (SUB; red) along the proximodistal axis (top) and a flat map showing tetrode positions in the CA1 and subiculum (bottom). The intermediate transition zone (SUB/CA1) is colored in white. Numbers on the left of the flat map indicate relative positions (mm) from bregma. Colored-dots represent tetrode positions for individual rats. A: anterior, P: posterior, M: medial, L: lateral. (B) Nissl-stained photomicrographs of the tissue sections that contained the tetrode trajectories marked by the arrows in (A).

Differences in firing properties between the CA1 and subiculum

As reported in prior studies (Barnes et al., 1990; Sharp and Green, 1994; Kim et al., 2012b), the mean firing rate was higher on average in the subiculum than in the CA1 ($Z = 6.83$, $P < 0.0001$, Wilcoxon rank-sum test) (**Figure 5**). In addition, units recorded from the CA1 burst more ($Z = 12.91$, $P < 0.0001$, Wilcoxon rank-sum test) and fired more spatially (spatial information score: 1.12 ± 0.06 in CA1, 0.25 ± 0.02 in subiculum; sparsity: 0.43 ± 0.02 in CA1, 0.78 ± 0.01 in subiculum; coherence: 1.81 ± 0.05 in CA1, 1.34 ± 0.04 in subiculum; spatial selectivity: 4.34 ± 0.18 in CA1, 2.14 ± 0.07 in subiculum; Mean ± S.E.M.; P-values < 0.0001, Wilcoxon rank-sum test) than the units recorded from the subiculum.

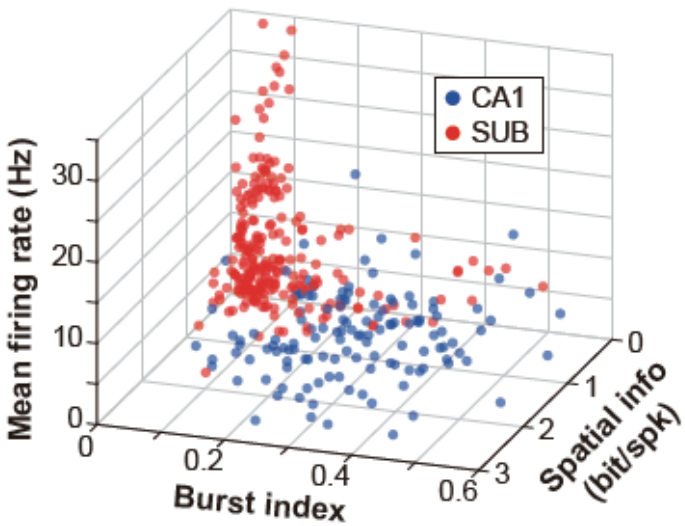

Figure 5. Basic firing properties of single units in the CA1 and subiculum. Note that CA1 (blue) and subicular (red) cells are well separated by firing properties. Only cells that passed the unit isolation criteria were used.

Single units in the CA1 and subiculum responded to task-relevant events

Subicular cells are known to show relatively poor spatial firing compared to hippocampal cells in general (Barnes et al., 1990; Sharp and Green, 1994), which was also the case in the current study. Therefore, I decided to organize the neural firing patterns by using the critical events that occurred in the task (Aronov et al., 2017), instead of using location-based neural representations. We named such a neural representation "*event rate map (ERM)*" in the current study. To construct an ERM, we defined three critical events associated with task demands as follows: *(a)* 'S' – opening of the door of the start box (which also corresponded to the onset of the scene stimulus, detected online by an optic sensor), *(b)* 'C' – choosing the left or right arm at the intersection (detected offline by calculating the position-diverging point), and *(c)* 'R' – displacing the disc that covered the food well containing reward (detected online by optic sensors) (**Figure 6A**). I also used the activities from three additional sensors and the bisecting point between the choice point and reward location as minor events to construct individual ERMs. Therefore, an ERM is composed of seven time points associated with the abovementioned seven events and the six event epochs between those time points (**Figure 6B**). Constructing an ERM enabled us to analyze the neural firing patterns recorded immediately before and after the door-opening event in the start box (which coincided with the onset of a scene stimulus) while capturing the spatial firing characteristics at the same time (**Figure 6C**).

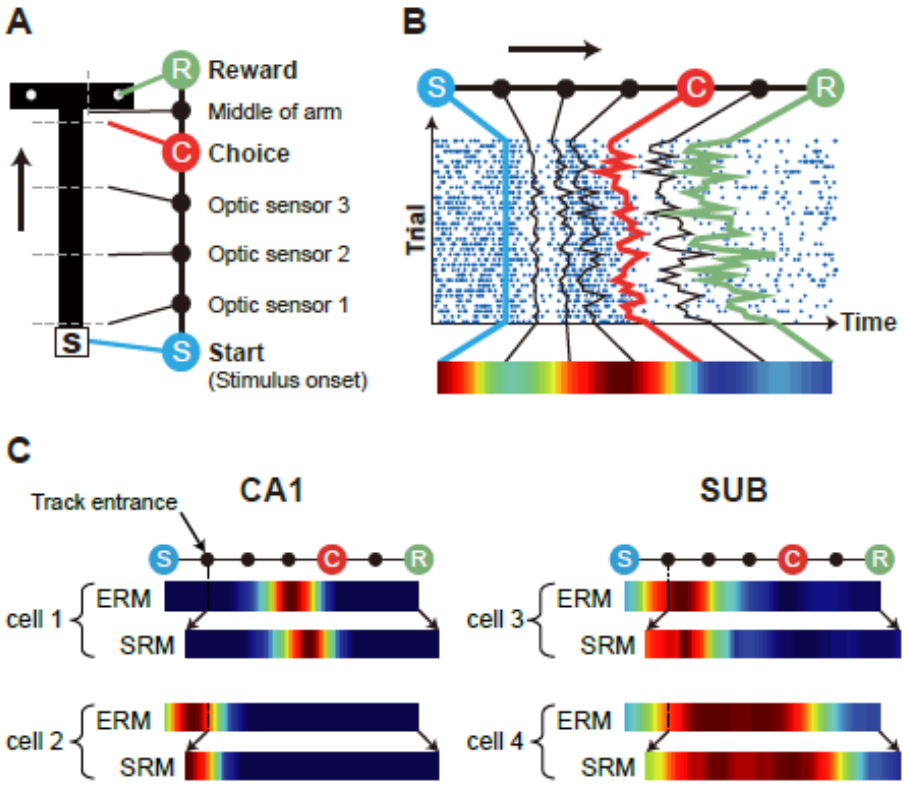

Figure 6. Basic firing properties of single units in the CA1 and subiculum. (**A**) Major events in the VSM task. The opening of the start box door (S), turning to the left or right arm at the choice point (C), and reaching the reward location (R) were defined as three major events. Three sensor-crossing points in the stem and bisecting point of each arm were minor events. The arrow denotes the running direction. (**B**) Event rate map (ERM). The raster plot of a single unit is used to as an example to illustrate how spiking activities were grouped into discrete event epochs to result in the ERM. (**C**) Examples of the event rate maps (ERM) and spatial rate maps (SRM) of cells in the CA1 and SUB. The epoch between the opening of the start box and track entrance was not represented in

the spatial rate map because the associated position data were not recorded in the start box in our experimental settings, whereas the event rate map could represent neural activity in the entire task period (including the neural activity inside the start box). Although the information-organizing schemes were different between the event rate map (time) and spatial rate map (location), both formats were very similar because time and location were highly correlated in our task on the maze.

Examining the individual ERMs of the CA1 and subiculum showed some differences between the two areas. Specifically, most units in the CA1 showed a single field occupying a narrow zone seemingly corresponding to the size of a single event epoch in the ERM ('SF' in Figure 7A). Some units fired at multiple epochs in the ERM in the CA1 ('MF' in Figure 7A) although there were not many such cases. In contrast, subicular units tended to fire across contiguous epochs in the ERM, resulting in longer single firing fields ('SF' in Figure 7B) or, when firing in multiple epochs separated from each other, multiple firing fields ('MF' in Figure 7B). In some units, we could not detect event-related fields (event-unrelated units; see Materials and Methods) and those units were excluded from analysis in the current study. Most CA1 units showed single fields (> 80%), whereas the units exhibiting single fields and multiple fields were almost equally found in the subiculum ($\chi^2_{(1)} = 49.69$, $P < 0.001$, Chi-square test) (Figure 7C). The sizes of event-related fields in the CA1 and subiculum were also statistically different from each other ($\chi^2_{(2)} = 75.92$, $P < 0.0001$, Kruskal-Wallis test; inset in Figure 7D). Specifically, the size of single fields in the CA1 was significantly smaller than that of the single fields in the subiculum (SF: $Z = 8.09$, $P < 0.0001$; single fields within MF: $Z = 2.63$, $P < 0.01$; Wilcoxon rank-sum test), and single fields in the subiculum were larger than the individual fields of the multiple fields in the subiculum ($Z = 7.27$, $P < 0.0001$).

Interestingly, the proximal region of the subiculum contained

more multiple-field units than single-field units and vice versa in the distal subiculum ($Z = 2.16$, $P = 0.033$, Wilcoxon rank-sum test) (**Figure 7E**). These might be attributable to the fact that the distal portion of the subiculum receives stronger inputs from the medial entorhinal cortex, whereas the proximal subiculum receives more inputs from the lateral entorhinal cortex (Cembrowski et al., 2018).

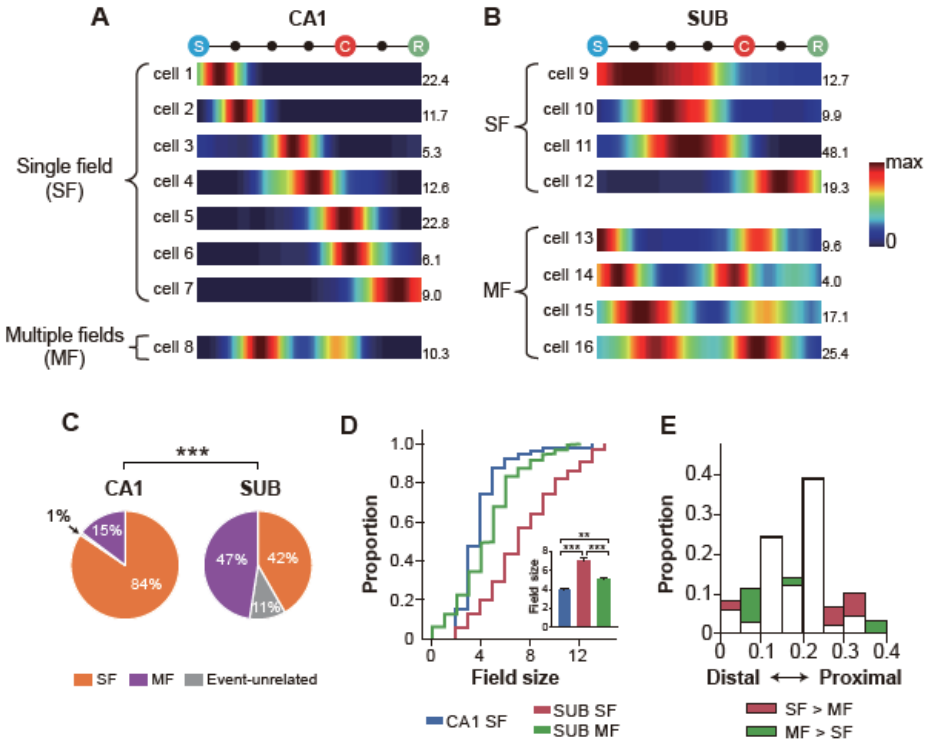

Figure 7. Types of firing fields in the CA1 and subiculum. (A and B) Representative ERMs in the CA1 (A) and subiculum (B). Numbers indicate the maximal firing rates. The color bar denotes the color scale for firing rate (max: maximal firing rate). (C) The proportion of single- and multiple-field types in the CA1 and subiculum. ***P < 0.001. (D) Comparison of the field sizes of the units with single fields and multiple fields in the CA1 and subiculum. Inset: Same data presented as bar graphs. Median ± 95% confidence interval/2. **P < 0.01, ***P < 0.001. (E) Histograms to compare the proximodistal distributions of single-field units with multiple-field units in the subiculum. Overlapping areas between single- and multiple-field distributions are colored in white. Note the presence of more multiple-field units in the distal subiculum (green areas) and more single-field units in the proximal subiculum (red areas).

Neurons in both CA1 and subiculum were equally capable of representing visual scenes differentially using rate modulation

I examined whether scene-dependent rate remapping also occurred in the subiculum when facing different visual scenes as previously reported in the dorsal CA1 (Delcasso et al., 2014). Because no significant difference was found during analysis between the single-field and multiple-field types in the subiculum, all ERMs were used in the subiculum for analysis. Confirming our prior findings (Delcasso et al., 2014), in the VSM task, some units in the CA1 exhibited robust rate remapping according to the rat's choice response (**Figure 8A**, cells 4-6). In contrast, other units' firing rates were modulated by visual scenes (when comparing between different scenes associated with the same choice response) (**Figure 8A**, cells 7-9). Importantly, similar rate remapping patterns were also found in the subiculum. That is, some subicular neurons changed their firing rates according to the rat's choice (**Figure 8B**, cells 13-15) and other units were more tuned to the visual scenes (**Figure 8B**, cells 16-18). In both regions, some cells were not responsive to task demands ('nonspecific units' in **Figures 8A** and **8B**).

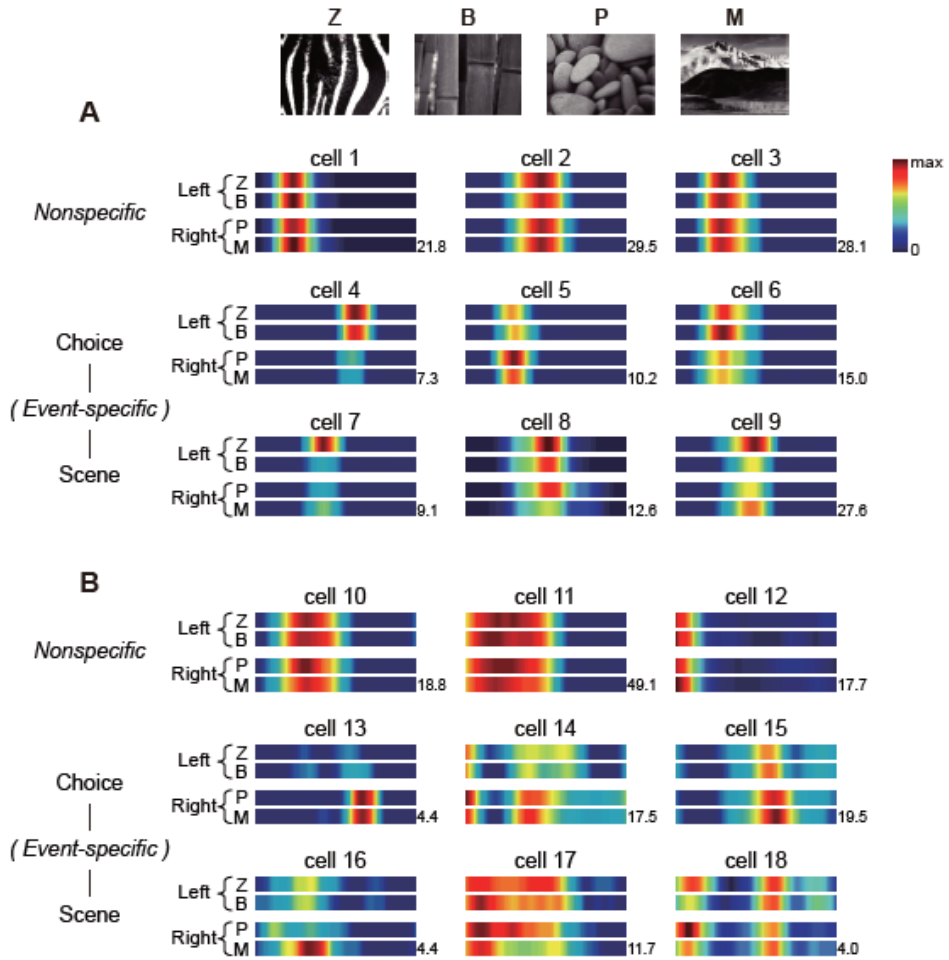

Figure 8. Task-dependent rate remapping in the CA1 and subiculum. (A and B) Representative ERMs of CA1 (A) and subicular (B) cells, associated with four scenes (Z: zebra stripes, B: bamboo, P: pebbles, M: mountains). Cells are sub-categorized into nonspecific, choice-specific and scene-specific units. Scene and associated spatial choice are labeled on the left side of each ERM. The number at the end of the ERM of each cell denotes the maximum firing rate.

To measure the amount of rate remapping, a rate difference index (RDI) was developed as follows. The RDI between the two choices (RDI_{CHOICE}) was obtained by calculating the absolute difference between the firing-rate distributions associated with the left-choice and right-choice trial types (i.e., FR_{LEFT} or FR_{RIGHT}) (**Figure 9A**). The RDI between the visual scenes within the same response type (e.g., zebra stripes and bamboo scenes for the left-choice trial type) (RDI_{SCN}) was obtained by calculating the difference in the firing-rate distributions associated with those scenes (with the larger RDI taken between RDI_{SCN-L} and RDI_{SCN-R}) (**Figure 9B**). I found no significant difference between the CA1 and subiculum with respect to both RDI_{CHOICE} ($Z = 1.60$, $P = 0.11$, Wilcoxon rank-sum test) (**Figure 9C**) and RDI_{SCN} ($Z = 0.19$, $P = 0.85$) (**Figure 9D**). In addition, no significant difference was found in both RDI measures between the classes of units with single fields and multiple fields in the subiculum (RDI_{CHOICE}: $Z = 0.07$, $P = 0.95$; RDI_{SCN}: $Z = 0.19$, $P = 0.85$; Wilcoxon rank-sum test).

I also tested the possibility that the units recorded from the tetrodes located at the transition zone between the CA1 and subiculum (i.e., SUB/CA1) affected the RDI distributions. However, I found no significant difference between the CA1 and subiculum when running the same statistical tests after removing the units recorded from the SUB/CA1 (RDI_{CHOICE}: $Z = 0.41$, $P = 0.68$; RDI_{SCN}: $Z = 0.32$, $P = 0.75$; Wilcoxon rank-sum test). These findings strongly suggest that task-relevant information (i.e., scene and choice response) is represented robustly in both the CA1 and subiculum when rats perform the VSM task.

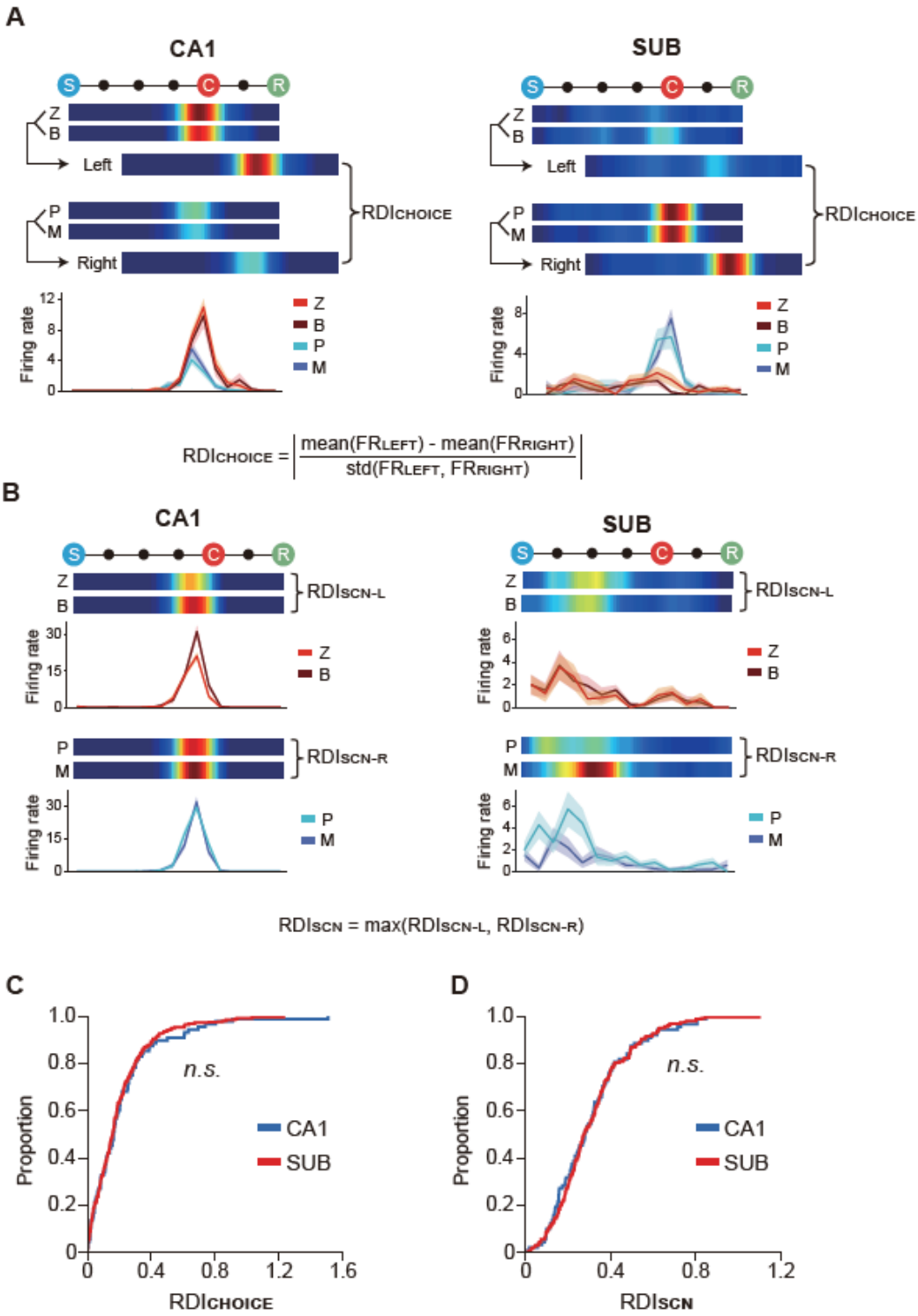
A
CA1
SUB
S
C
R
Z
B
P
M
Left
Right
RDIchoice
Firing rate
B
RDIscn-L
RDIscn-R
RDIchoice = |mean(FRleft) - mean(FRright) / std(FRleft, FRright)|
RDIscn = max(RDIscn-L, RDIscn-R)
C
D
Proportion
n.s.
CA1
SUB
RDIchoice
RDIscn

Figure 9. Comparison of rate remapping between the CA1 and subiculum. (A and B) Illustration of the procedures for calculating the rate difference index (RDI). Each panel consists of the ERMs associated with different task-relevant information (top) and line graphs that compare the firing rates between different scene conditions along the event axis (bottom). (A) Rate difference index for choice (RDI_{CHOICE}). Scenes associated with the same choice arm were combined to measure the field's firing rate for each side (i.e., FR_{LEFT} and FR_{RIGHT}). RDI_{CHOICE} is the difference between the firing rates associated with the left and right choices. (B) Rate difference index for the scene (RDI_{SCN}). RDI_{SCN-L} and RDI_{SCN-R} are RDI values computed for different scenes that share the common choice arm, and the larger of the two was taken as RDI_{SCN} of the unit. (C and D) Cumulative distributions of RDI_{CHOICE} (C) and RDI_{SCN} (D). RDI_{CHOICE} was not significantly different between the CA1 and subiculum, and the same was the case for RDI_{SCN}.

Discussion

Previous studies have reported that cells in subiculum exhibit relatively broad firing fields and poor spatial tuning compared to the narrow and spatially selective firing patterns of CA1 place cells (Barnes et al., 1990; Sharp and Green, 1994). The differences in firing characteristics made it difficult to compare the firing fields between the two regions, and to find the subregional differences by the conventional spatial analysis. Therefore, in the current study, ERM was constructed by organizing the firing activities using task-relevant events. Additionally, field boundaries were defined by increase or decrease of firing rates to cope with the firing patterns in the subiculum, which has a lower minimum-to-maximum ratio than those in CA1. Then, it was tested whether visual scene is represented by the firing rate modulation within the subicular firing fields.

As a result, I observed that the subicular firing fields had the following characteristics: (1) Subicular single field (SF) is distributed over wider events compared to CA1, (2) A much larger proportion of cells have multiple fields (MF) compared to CA1, and (3) Approximately 10% of the subicular cells have no field due to spatially continuous firing activity (event-unrelated). Furthermore, I found rate modulation representing task-specific information in the individual firing fields of the subiculum, and found that the degree of rate modulation is similar to that of CA1.

However, there were still limitations in interpreting subicular firing activity by analytical methods using ERM. First, ERM has lower resolution than SRM. In this experiment, the interval between the task-relevant events used to make the ERM was not controlled. Therefore, the interval between the events is very short. While this is advantageous for observing firing patterns based on task-relevant events, it can be difficult to analyze the firing activity in detail. The second is that it still depends on the firing rate. Cells in the subiculum, unlike those in the CA1, exhibit a strong spontaneous firing activity and tends to have place fields with a low peak firing rate. Therefore, it might be that a latent firing field was undetected.

In order to overcome these limitations of ERM, Experiment 2 adopted a new analytic method that additionally used spiking phase as well as spiking frequency in spatial dimension.

EXPERIMENT 2. Representation of Visual Scene in the CA1 and Subiculum after the Theta Phase-based Parcellation of Spiking Activities into Place Fields

Introduction

Hippocampal place cells exhibit a well-known temporal coding phenomenon called ‘theta phase precession (O'Keefe and Recce, 1993). Theta phase precession is a phenomenon in which the cell's spiking phase relative to LFP theta oscillation gradually shifts to an earlier phase when the rat passes through the cell’s place field. In a previous study, two or more overlapping CA1 place fields were successfully separated using such spiking-phase relationships (Maurer et al., 2006). Thus, it was suggested that spiking phase is critical for detecting a unitary place field.

Spiking phases can be particularly useful when dealing with subicular firing activities because of their low signal-to-noise ratios. A recent study, which reported that theta phase precession also appears clearly in the subiculum (Kim et al., 2012b), defined multiple place fields in the subiculum by developing an automatic algorithm that detects phase precession cycles. However, only a few examples were shown regarding how the subicular place fields was defined in that study, which makes it difficult to confirm the validity of the method. In addition, actual subicular firing patterns were so complex to find the boundaries of place fields using a fully automatic algorithm. And the following issue has to be considered in our VSM task: the place field might have cancelled out in the averaged firing rate map due to rate-remapping induced by environmental changes across trials.

To address these issues, I devised a new analytical method to find spike clusters composing phase precession cycles by applying an existing clustering algorithm called DBSCAN (density-based spatial clustering with application of noise). Then, it was examined whether the phase code is efficient for finding latent place fields in the spontaneous firing activities of the subiculum. Finally, I retested whether there were changes in the degrees to which subicular neurons represented visual scenes compared to the previous results based on just event rate-based analysis in Experiment 1.

Methods

Speed filtering

For spiking phase analysis, only epochs when the rats were running over a certain speed were used to detect theta oscillation more clearly. In order to obtain the instantaneous running speed, the linearized position data recorded at 30 Hz was smoothed in two steps. First, linear interpolation was applied to compensate for vacancies of the position data caused by the rats' head movement or tether interference. Next, outlier data points were suppressed using a robust locally weighted regression. Then, I divided the length of the three consecutive points by the duration of time to calculate the instantaneous running speed, and assigned the speed value to the middle point of the three. The average running speed was 35.3 cm/s in all sessions of all rats. Spikes that occurred while the running speed was above 20 cm/s were used in this experiment. Trials in which the latencies from start box to foodwell were longer than 6 s were discarded.

LFP analysis

Pre-processing

Local field potential (LFP) was down-sampled from 32 kHz to 2 kHz and filtered in the theta (8-12 Hz) range using zero-phase bandpass filter (3rd-order Butterworth filter with 'filtfilt' function in MATLAB). The reason for filtering to the high theta frequency band is to eliminate the bumping noise that occurred when the rats' heads

hit the start box door or track walls. LFP traces from running epochs were visually inspected to exclude tetrodes whose voltage traces exceeded the maximum value of AD converter or frequently generated artifacts such as bumping noise.

Channel selection

A power spectral density (PSD) function was obtained by a multi-taper method (Chronux ToolBox; MATLAB). Then, theta band power of each tetrode was estimated to obtain the ones with the strongest theta power as a reference channel for the session. LFPs recorded from the CA1 and subiculum were used to obtain spiking phases of CA1 and subicular cells, respectively.

Spiking theta phases

The Hilbert transform was used to decompose the LFPs into amplitude and phase information (Harris et al., 2003). To examine the spiking-phase relationships, the instantaneous theta phases and linearized positions corresponding to the timestamps when the spikes were generated were plotted on a 2-dimensional space (phase-position plot).

Identification of place fields using DBSCAN

To capture the groups of spikes surveying the same spiking-phase relationship, I adopted a commonly used clustering algorithm called DBSCAN (density-based spatial clustering of applications with noise) (Ester et al., 1996). DBSCAN is a density-based, non-parametric

algorithm that clusters points gathered in close proximity in space, while excluding distant or sparsely located points as noise. It is not necessary to specify the number of clusters in advance, but some parameters must be determined to run this algorithm: distance ε and minimum number of points N_{min}. Specifically, if the number of data points in distance ε from a point is greater than N_{min} including itself, it is defined as a core point of a cluster. If another point contains the core point within distance ε but does not satisfy N_{min}, it is defined as a border point. If there is no core point and N_{min} is not satisfied, the point is defined as a noise point (**Figure 11A**). In the current procedure, by adding the total number of points in a cluster as a parameter, only clusters with a certain number of points or more were considered valid. Those parameters were determined manually, so that the number of clusters in a cell was greater than the number of local maxima observed in the linearized firing rate maps. In order to prevent biased clustering arisen from experimenter's subjectivity, cross-validation was performed with three additional experimenters that were behind the procedures.

Cluster quality measurements

To estimate whether the spike clusters were well- or poorly-separated, two quality measurements were calculated for individual clusters: L-ratio and isolation distance (Schmitzer-Torbert et al., 2005). These two quality measurements are based on Mahalanobis distance $D_{i,C}^2$ of the spike i from the center of the cluster C, which is defined on the eight dimensional space (4 channels of tetrode × 2

features) using energy and the first principle component of the waveforms. L-ratio of cluster C is calculated as:

$$\mathrm{L(C)} = \frac{\sum_{i \notin C} 1 - CDF_{\chi^2_{df}}(D^2_{i,C})}{n_C}$$

where $i \notin C$ is a group of spikes not belonging to the cluster C, $CDF_{\chi^2_{df}}$ is the cumulative distribution function of χ^2 distribution with eight degree of freedom (df), n_C is the total number of the spikes in the cluster C. Low value of L-ratio means that the waveforms of the spikes in the cluster share similar features and well-separated. Isolation distance is the D^2 of the $n_c th$ closest noise spike, which means higher value of isolation distance indicates that the cluster C is more distant from the other spikes.

Clusters satisfying L-ratio > 0.02 and isolation distance < 14 were determined to be poorly-separated. Cells whose number of poor clusters accounted for more than half of the total number of clusters were excluded from the analysis.

Theta phase precession

After the parcellation of unitary place fields in the theta phase-based manner, the group of spikes were fitted by a linear regression line to identify significant phase shifts. Theta phase precession of a place field was considered significant if the following criteria were achieved: (1) The range of phase shifts $\geq 180^\circ$, (2) The slope of regression line is negative, and (3) The measurement for goodness-of-fit $\geq$ 0.01.

Results

Theta phase precession in the subiculum

I first confirmed that the spiking activities of the subiculum were modulated by local theta oscillation. Theta rhythms were obtained from local field potential (LFP) filtered in the high theta frequency band (8−12hz) to avoid artifact signals such as bumping noise (Figure 10A). Theta phase and linearized position corresponding to each spike were calculated and plotted in a 2 dimensional space (Figure 10B). In this phase−position plot, I observed theta phase precession clearly in the subicular place field. Therefore, it was thought that the place field could be defined by clustering a group of spikes generated from a single cycle of phase shift.

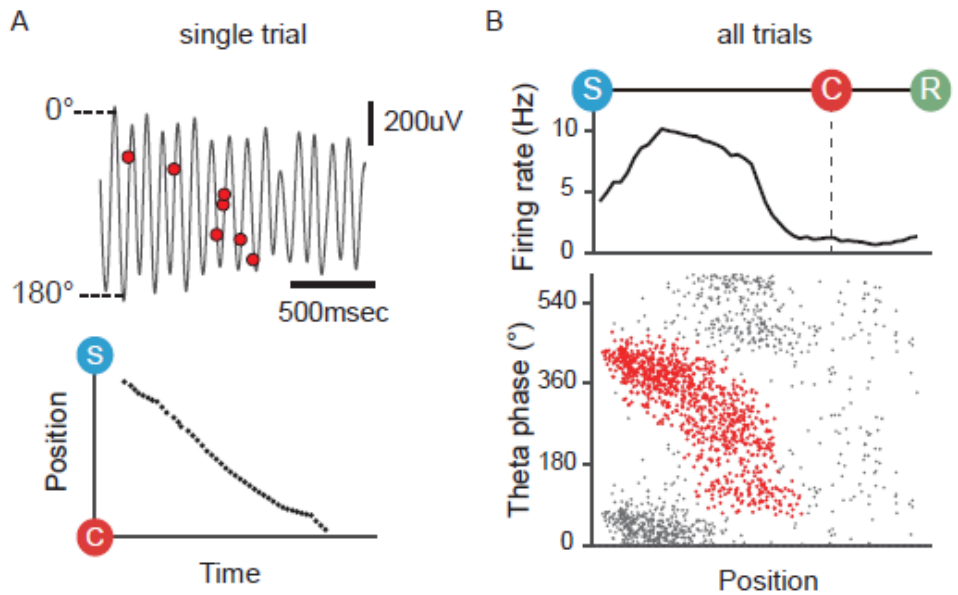

Figure 10. Theta phase precession clearly observed in the subiculum. (A) Theta phase precession in a single trial. Theta-band filtered local field potential in the subiculum overlapped with the spiking activities recorded at the same time (top) and the position trace as a rat ran through the stem of the track (bottom). (B) Theta phase precession occurred in the subiculum. Linearized firing rate map across a session (top) and phase-position plot (bottom). Theta phases of all spikes in the session plotted as a function of position. Red dots indicate spikes occurred in a firing field. Black dots indicate spikes outside the firing field. The phase-position plot is duplicated to show the phase-periodicity. Vertical dashed line denotes spatial choice point.

Identification of subicular place fields based on theta phase in the application of DBSCAN algorithm

To capture the spike clusters comprising a theta phase precession observed in the phase–position plot, an existing algorithm called DBSCAN (density–based spatial clustering with applications of noise) was employed (Ester et al., 1996). DBSCAN is a clustering algorithm that finds spatially dense parts. It is a semi–automatic method in which the experimenter has to decide some parameters in advance. Specifically, it is necessary to determine distance ε from a data point and minimum number of points N_{min} within distance ε (**Figure 11A**, see Materials and methods for details). This algorithm has been chosen because of its several advantages. Assuming sufficient sampling, spikes occur in a place field with the highest probability at the most preferred location and gradually diminish as the distance from the center increases like Gaussian–like distribution. DBSCAN, the density–based protocol, is suitable for finding clusters with such distribution. The DBSCAN algorithm also has the advantage of robust detection of outliers, which enables us to deal with continuous and spontaneous firing activities of the subicular fields. Finally, this algorithm does not need to determine the number of clusters in advance, and the form of the cluster is not limited, so it is highly flexible.

In the previous study of Kim and colleagues, they normalized the phase–position plot by the rat's occupancy to construct a phase–position firing–rate map, and detected local maxima to define the

firing fields. However, they used a behavioral paradigm in which rats just run along the track without cognitive process induced by environmental changes or behavioral responses. On the other hand, in the current study, cells in the subiculum were expected to exhibit rate modulation in their firing fields due to the scene stimulus presented differently trial by trial and its associated choice response. Occupancy normalization applied to phase-position plot might be cancel out these potential firing fields (**Figure 11B**). Therefore, the clustering algorithm was performed to the raw phase-position spike plot without occupancy normalization.

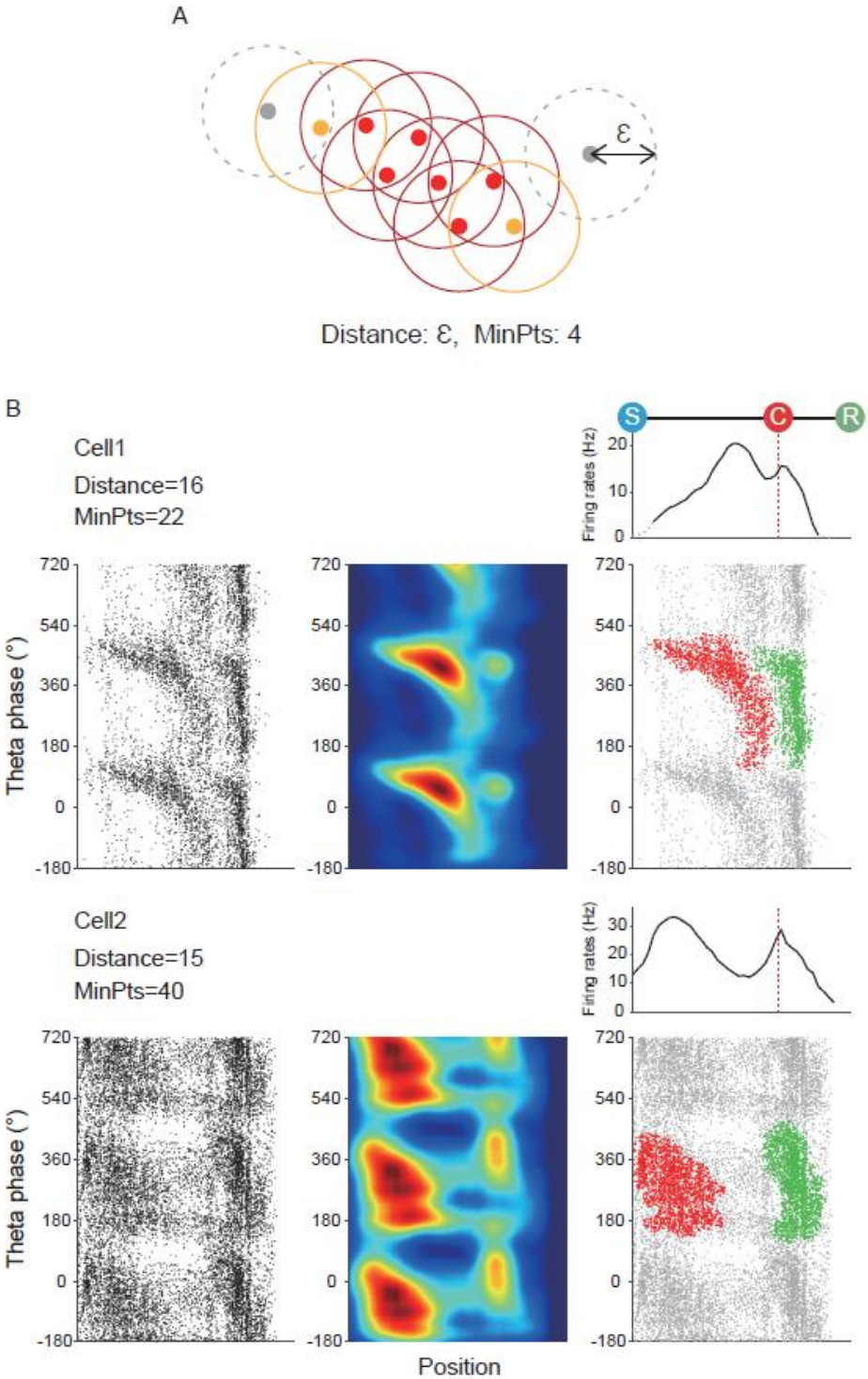
A
ε
Distance: ε, MinPts: 4
B
Cell1
Distance=16
MinPts=22
S
C
R
Firing rates (Hz)
20
10
0
Theta phase (°)
720
540
360
180
0
-180
Cell2
Distance=15
MinPts=40
30
20
10
Position

Figure 11. DBSCAN algorithm used for detection of place fields.

(A) Illustration of how DBSCAN algorithm works. Red dots for core points, orange dots for border points, and gray dots for noise points. A cluster consists of core points and border points, excluding noise points. (B) Two example subicular cells applied with DBSCAN algorithm. First column shows raw phase-position plots for each cell before clustering. Second column is for phase-position firing-rate maps normalized by occupancy of the rat. Third column shows linearized firing rate maps (top) and color-coded spike clusters parsed by DBSCAN algorithm (bottom). Note that phase-position firing-rate maps are not enough to capture the entire forms of spike clusters which are detected on the un-normalized phase-position plots.

Since DBSCAN is very flexible in defining clusters, it is possible that clustering is done in an artificial form. In order to screening such poor clustering, isolation distance and L-ratio are introduced as cluster quality measurements. The clustering quality criteria were determined by visual inspection of cells with poor clustering results. Clusters satisfying L-ratio > 0.02 and isolation distance < 14 were determined to be poorly-separated (read area in **Figure 12A**). These criteria were good at filtering out the abnormal and irregular form of clusters (**Figure 12B**). Cells whose number of poor clusters accounted for more than half of the total number of clusters were excluded from the analysis (**Figure 12C**; n=3 for single-fields in CA1, n=14 for multiple-fields in CA1, n=9 for single-fields in SUB-SF, n=64 multiple-fields in SUB).

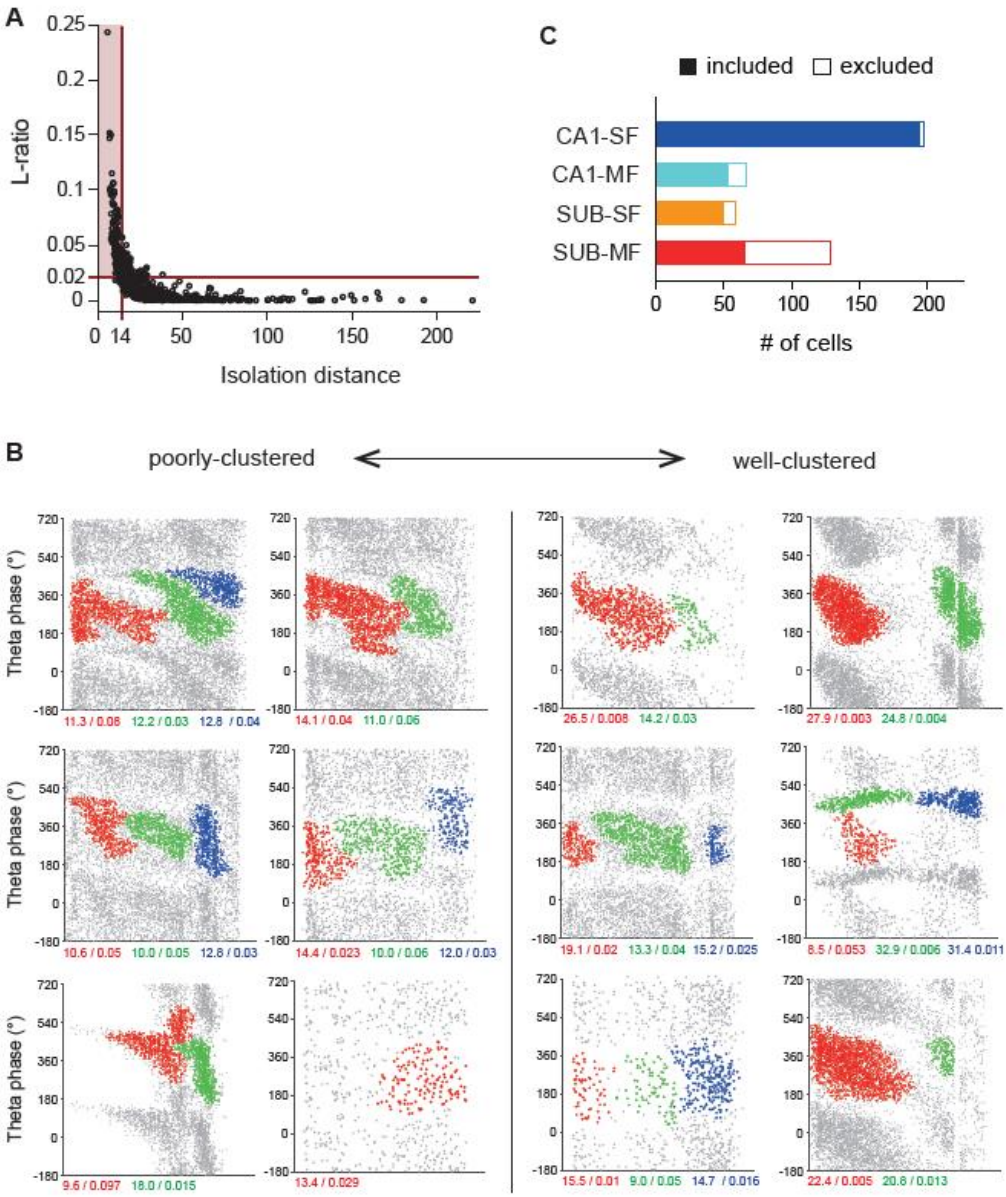
A
L-ratio
0.25
0.2
0.15
0.1
0.05
0.02
0
0 14 50 100 150 200
Isolation distance
C
included
excluded
CA1-SF
CA1-MF
SUB-SF
SUB-MF
0 50 100 150 200
# of cells
B
poorly-clustered
well-clustered
Theta phase (°)
720
540
360
180
0
-180
11.3 / 0.08 12.2 / 0.03 12.8 / 0.04
14.1 / 0.04 11.0 / 0.06
26.5 / 0.008 14.2 / 0.03
27.9 / 0.003 24.8 / 0.004
10.6 / 0.05 10.0 / 0.05 12.8 / 0.03
14.4 / 0.023 10.0 / 0.06 12.0 / 0.03
19.1 / 0.02 13.3 / 0.04 15.2 / 0.025
8.5 / 0.053 32.9 / 0.006 31.4 0.011
9.6 / 0.097 18.0 / 0.015
13.4 / 0.029
15.5 / 0.01 9.0 / 0.05 14.7 / 0.016
22.4 / 0.005 20.6 / 0.013

Figure 12. Validity of clustering tested by quality measurements. (A) Distribution of isolation distance and L-ratio of all individual clusters detected from the CA1 and subiculum. Red lines indicate the criteria of clustering quality. Dots in the red area are determined to be poor clusters. (B) Examples of subicular cells that are poorly- or well-clustered. Numbers below the phase-position plots denote the isolation distance and L-ratio of individual clusters. Cells with poor quality for more than half of the clusters were excluded from further analysis. (C) Summary of cluster validity screening. Bar graphs showed the number of poorly- and well-clustered cells for each type of firing fields.

Latent place fields detected by theta phase-based clustering in the CA1 and SUB

By applying the clustering algorithm described above, the latent place fields were defined based on theta phase of spiking. I compared how this theta phase-based fields (TP-based) differ from the fields defined using firing rate (FR-based). CA1 cells usually had a single field where theta phase precession clearly appeared (cell1-2 in **Figure 13**). However, some CA1 cells that exhibited a single FR-based field, changed to have multiple TP-based fields (cell3-4 in **Figure 13**). In the subiculum, some cells showed single TP-based fields similar to CA1 place cells (cell1-2 in **Figure 14**), but a number of cells showed multiple TP-based fields with repeated cycles of theta phase precession (cell3-7 in **Figure 14**). Note that these multiple TP-based fields observed in the subicular cells were originally defined as a single FR-based. In some cases, latent fields that were undetected due to the low firing peak were discovered together with the existing fields (cell4-7 in **Figure 14**). Additionally, few cells exhibited no theta phase precession but separated multiple clusters on the phase-position plot (cell8 in **Figure 14**).

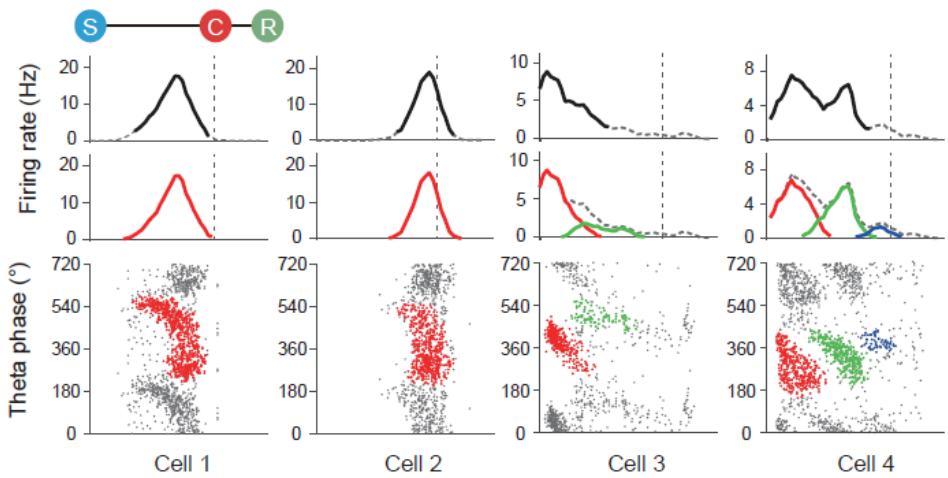

Figure 13. Examples of TP-based place fields in the CA1. (Top) FR-based firing fields. Bold lines are defined firing fields, while dashed lines are firing activities outside the firing fields. (Middle) TP-based firing fields. Color-coded lines depict individual firing fields, while dashed lines indicate overall firing activities. (Bottom) Phase-position plots duplicated over two cycles of theta to show the phase-periodicity. Individual spike clusters corresponding to the place fields are color-coded.

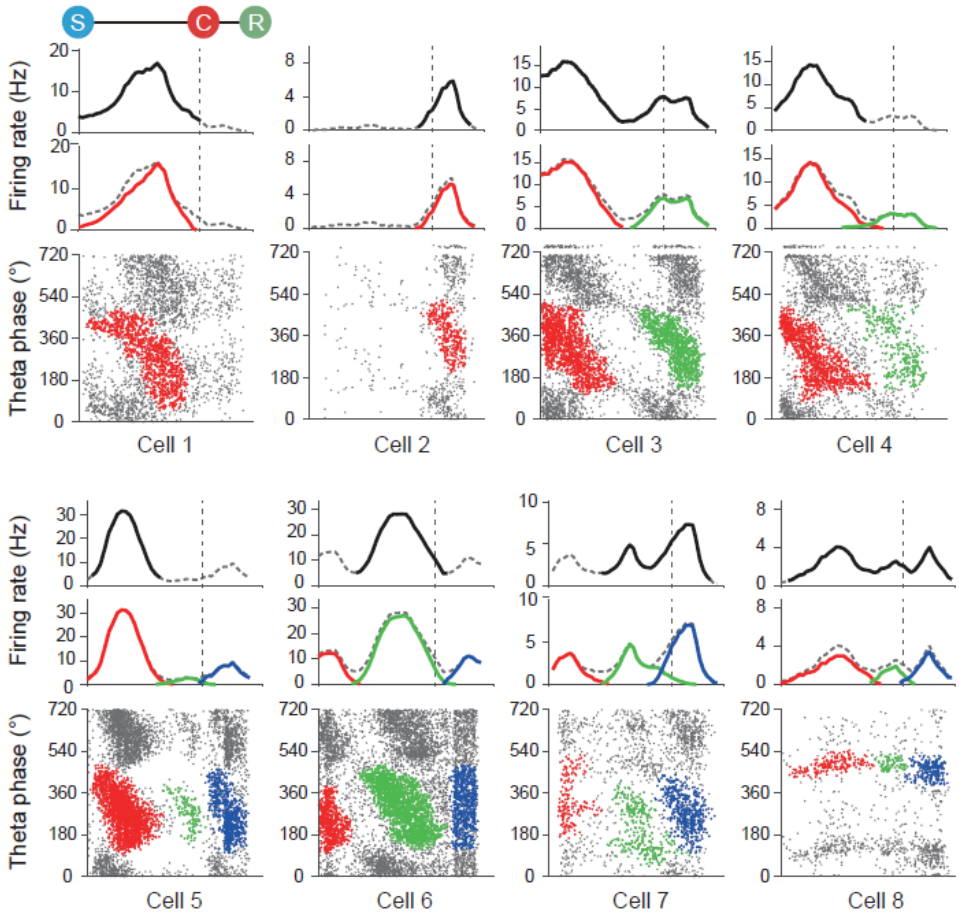

Figure 14. Examples of TP-based place fields in the subiculum. (Top) FR-based firing fields. Bold lines are defined firing fields, while dashed lines are firing activities outside the firing fields. (Middle) TP-based firing fields. Color-coded lines depict individual firing fields, while dashed lines indicate overall firing activities. (Bottom) Phase-position plots duplicated over two cycles of theta to show the phase-periodicity. Individual TP-based clusters are color-coded.

Moving from the FR-based method to the TP-based method, the firing field numbers and firing properties of CA1 and SUB cells were changed. 194 CA1-SF units, 53 CA1-MF units, 50 SUB-SF units, and 65 SUB-MF units were used for analysis. In CA1, about 20% of cells that had FR-based single field were changed to have TP-based multiple fields, and in SUB, about 60% of cells were changed from single field to multiple fields (**Figure 15A**). Since the FR-based single field was divided into TP-based multiple fields in a large number of subicular cells, the median value of firing field size in the subicular single-field cells was significantly reduced after the TP-based clustering. But it was still larger than that of the CA1 cells and subicular multiple-field cells (**Figure 15B**). Compared to the significantly changed firing field sizes, there was no difference average firing rate within the place fields between FR-based and TP-based methods (**Figure 15C**). This result implied that the TP-based clustering did not seem to separate the firing activities in an artificial way.

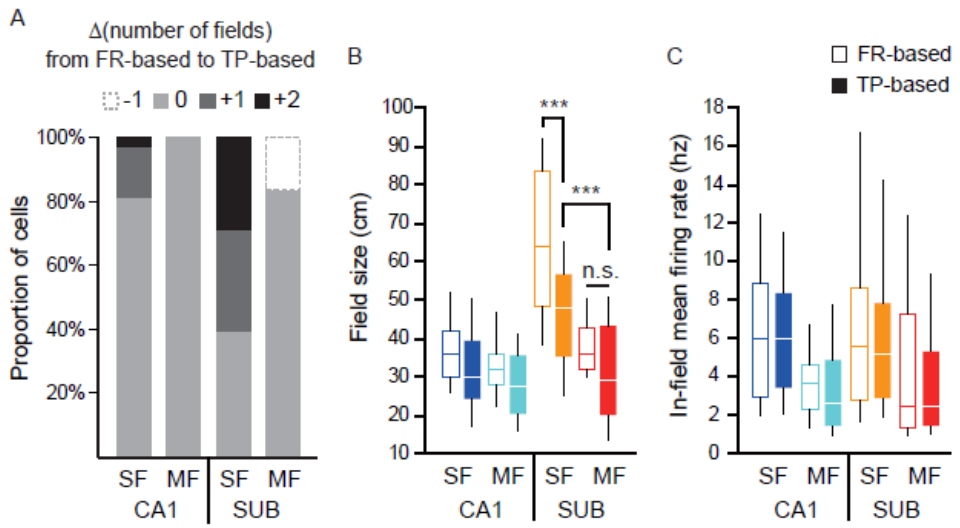

Figure 15. Changes in firing properties between FR− and TP−based firing fields. (A) Proportion of cells that changed their number of fields as the definition scheme of place fields was switched from FR−based to TP−based method. Approximately 20% of CA1 single−field (SF) cells and 60% of subicular single−field cells were transferred to multiple−field (MF) cells after the TP−based clustering. (B and C) Changes in place field size (B) and in−field mean firing rate (C) for each field type in the CA1 and subiculum.

The characteristics of theta phase precession observed in TP-based fields of CA1 and SUB were also examined. Among the quantified properties of theta phase precession by linear regression, if (1) the range of phase shift is over 180 degrees, (2) the regression strength is greater than 0.01, and (3) the regression line has a negative slope, I defined that the place field has a significant theta phase precession. As a result, 80-88% of single-fields in the CA1 and subiculum showed significant phase shifts, whereas only 51-58% of multiple-fields in both regions did so (**Figure 16A**). The initiating theta phase of individual phase precession was around 180 ° for single-fields of CA1 and around 90° for CA1 multiple-fields and subicular place fields (**Figure 16B**). Finally, the slope of theta phase precession was generally steeper in the CA1 (**Figure 16C**), consistent with previous literature reporting that the slope of phase shift is correlated inversely with the field size (Huxter et al., 2003).

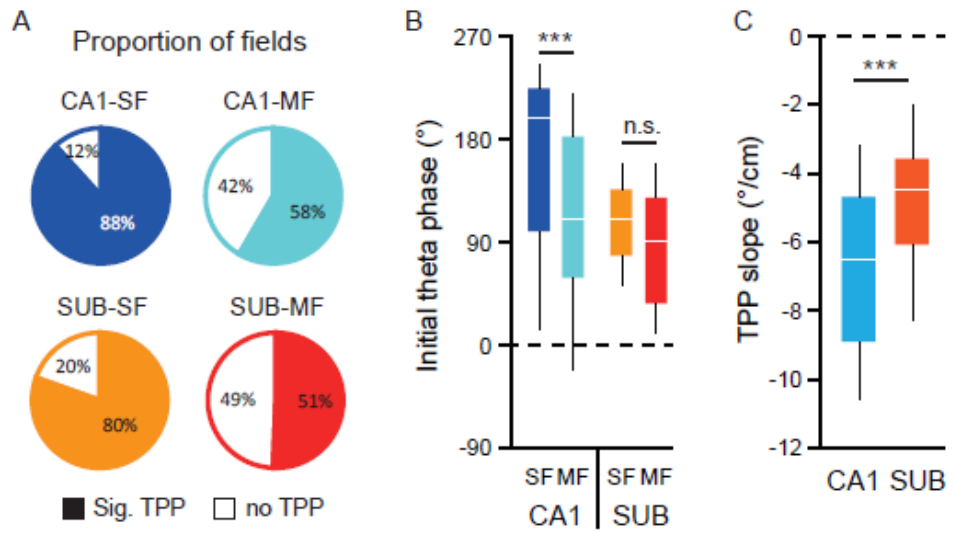

Figure 16. Differences in properties of theta phase precession between the CA1 and subiculum. (A) Proportion of place fields showing significant theta phase precession. Only the fields with significant phase precession was used for property analysis. (B) Distribution of initial theta phases for each field type in the CA1 and subiculum. (C) Differences in the slope of theta phase precession between the CA1 and subiculum.

Task-dependent rate remapping

We investigated how theta phase-based parcellation of firing activities influenced the scene representations of the CA1 and subiculum. In particular, when the cells having a single field based on the FR-based analysis are divided into multiple fields by TP-based clustering, the task information represented in the FR-based single field might be divided into different sub-fields (**Figure 17**). I found that the TP-based place fields of CA1 and subiculum tended to increase degree of rate modulation compared to FR-based fields. This is presumably due to the fact that the pattern of rate modulation, which was formed in different sub-fields, was canceled out in one continuous field.

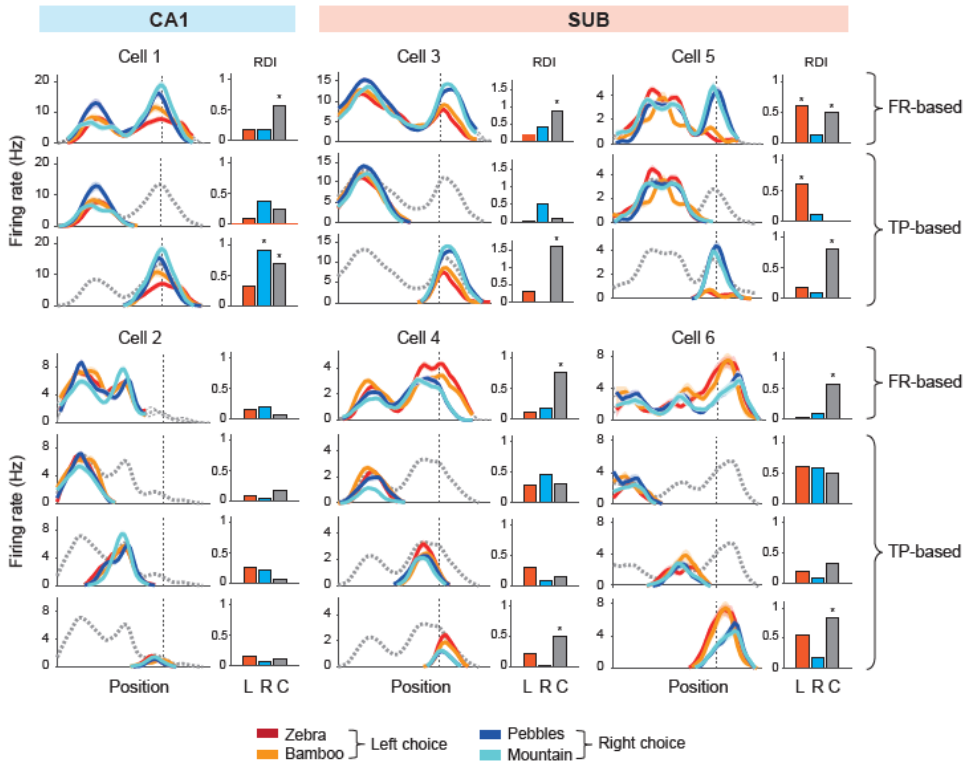

Figure 17. Task-dependent rate-remapping in the TP-based firing fields. To find changes in the distribution of task-dependent information, rate modulation index (RDI) was calculated for both FR-based and TP-based fields within a cell. The first panel of each cell is for FR-based firing fields and the panels below are for TP-based firing fields. Line graphs are color-coded to compare the firing activities between different scene stimuli. Bar graphs indicate RDI values between left-choice scenes (orange), right-choice scenes (blue), and choices (gray) respectively (L: RDI_{SCN-L}, R: RDI_{SCN-R}, C: RDI_{CHOICE}).

Discussion

To address the limitations of the conventional spatial analysis that defines hippocampal place fields based on firing rate, we tried to define place fields by extracting spike clusters with homogeneous spiking–phase relationships. In this way, it was possible to derive latent place fields from a broad and continuous firing activities in the CA1 and subiculum. In addition, I found that these fragmented fields represent different non–spatial information. Therefore, it can be suggested that the combination of temporal code and rate code should help to interpret seemingly noisy firing patterns of the subiculum. Furthermore, multiple fields were observed more frequently by theta phase–based clustering in the CA1 as well, suggesting a new analytical paradigm for CA1 place cell–related electrophysiology studies that still depend on firing rate.

General Discussion

In the current thesis, I have reported some differences in neural firing correlates between the CA1 and subiculum. Despite these differences, neurons in both CA1 and subiculum showed similar amounts of rate remapping between different scenes when rats were tested with visual scenes.

Prior studies also reported the relatively broad fields in the subiculum (Barnes et al., 1990; Sharp and Green, 1994), but their functional significance has been unclear. Our study implies that task-related information represented by the focal fields in the CA1 may be packaged in the subiculum into more schematic firing fields matching the critical epochs (e.g., pre- and post-choice periods). The fact that those broadly tuned cells in the subiculum conveyed scene and choice information as robustly as CA1 cells suggest that the schematic firing patterns in the subiculum may not simply stem from poor spatial firing properties. Such interpretations are also supported by the similarity within the same epoch as well as the orthogonality between different epochs in the task, both simultaneously observed in the neuronal population in the subiculum. Theoretically, it may not be necessary for an action system downstream of the hippocampus to know where in the maze a certain scene was experienced with the greatest precision to determine its final action because a background scene is supposed to remain unchanged in a certain area in the environment. According to this scenario, the task epoch-based

chunking in the subiculum might be a more practical way of processing information in the downstream regions (especially for action systems) of the hippocampus. The hippocampus may need to monitor contextual information with finer resolutions in space compared to other areas because a novel significant event may occur at any point in time and space (Knight, 1996; Vinogradova, 2001). This speculation may be connected to the phenomenon that subicular cells fired similarly when the rat experienced two adjacent chambers of different shapes (Sharp, 1997) although CA1 neurons tended to remap in those situations.

How does such a broadly tuned field arise in the subiculum when its immediate upstream structure exhibits spatially focal fields? One possibility is that efferents of multiple cells in the CA1 may converge onto a single neuron in the subiculum (O'Mara et al., 2009). If multiple afferent cells in CA1 have adjacent or partially overlapping fields, it may result in a broad single field in the receiving subicular neuron. Likewise, a subicular neuron may exhibit multiple fields if its afferent cells have non-overlapping fields. Another possibility is that the broad subicular fields may be driven largely by the upstream neocortical regions (Agster and Burwell, 2013). For example, the firing fields of neurons in the perirhinal cortex tend to cover a large segment of the environment (Bos et al., 2017). However, the range of the coverage of the perirhinal fields appears to be much broader (e.g., an entire left arm of a modified T-maze) than those observed in the subiculum in the current task.

When examined at the population level, the neurons with single

fields in the subiculum appear to cover the critical epochs of the task in a schematic (or categorical) manner, as opposed to more specific location-bound fields in the hippocampus (Lee et al., 2018; Figure 18). In this study, the schematic coding could not be simply generated by large subicular fields in the present task, emphasizing the importance of some structured organization of the population representations reflecting task demands (Figure 19).

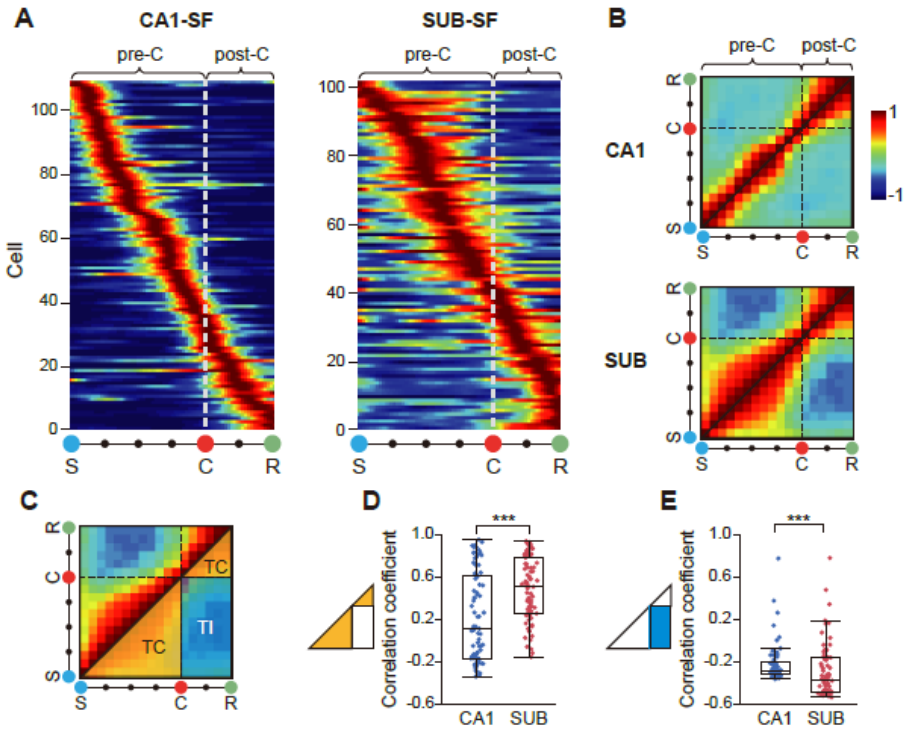

Figure 18. Schematic firing patterns of the neural populations in the subiculum, but not in the CA1. (A) Population ERMs for the CA1 and subiculum. Individual ERMs were aligned according to their maximal firing locations along the event dimension (S−C−R). The white dotted line denotes the boundary between the pre−choice (pre−C: S to C) and post−choice (post−C: C to R) periods. (B) Autocorrelation matrix showing the cross−correlations between the same population ERMs to reveal positively correlated (warm colors) and anti−correlated (cool colors) areas in the population ERM. Black dashed line: choice point. (C) Task−congruent (TC, orange triangles) and task−incongruent (TI, blue rectangle) areas in the autocorrelation matrix (only shown in the lower half of the matrix to avoid duplicate information). (D and E) Comparison of mean correlation coefficients between the CA1 and subiculum in the task−congruent area (D) and task−incongruent area (E). ***$P < 0.001$.

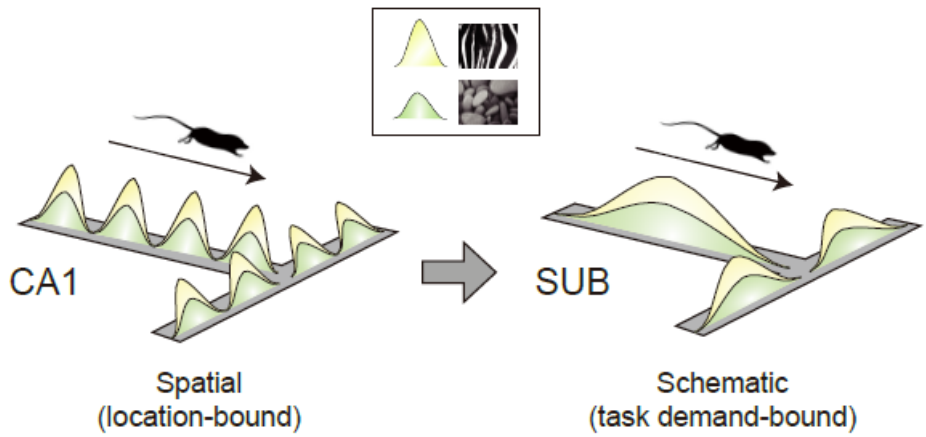

Figure 19. Illustration of the differential coding schemes between the hippocampus and subiculum. Location-specific firing patterns of CA1 cells are translated (by chunking) into schematic representations in the subiculum. Overlapping fields in different colors illustrate the scene-dependent rate remapping with each field associated with one of the visual scenes in the task.

Finally, the so-called axis-tuned cells in the subiculum (Olson et al., 2017) might underlie our findings because the pre-choice and post-choice epochs in our task roughly correspond to the vertical and horizontal axes of the T-maze, respectively. However, it is unlikely that the phenomenon reported here was mainly driven by axis-tuned cells in the subiculum. This is because there were approximately 8% of cells in the subiculum that were identified as axis-tuned cells according to the previous study (Olson et al., 2017), whereas over 40% of recorded units in the subiculum showed broad single fields in our study. Also, the single-field units in our study showed rate remapping according to the task-relevant information to the similar extent compared to CA1 cells, suggesting that the subicular cells may represent more complex task-specific components than a simple spatial component.

To our knowledge, the scene- and choice-dependent rate remapping of the subiculum in a memory task have never been reported. Together with the rate remapping previously observed in the CA1 and dorsomedial striatum in the VSM task (Delcasso et al., 2014), the subicular rate remapping reported here may support the idea that scene-dependent rate remapping may not be a unique code of the hippocampus. Instead, rate remapping may be a general code used across different areas. Subicular neuronal firing carried similar amounts of scene and choice signals compared to the hippocampal firing when the rat performed the overly trained task with the same scenes. However, introducing a novel task demand by intermixing blurred stimuli with the original ones altered the firing patterns of the

CA1 dynamically to reflect the physical changes in the scenes (Lee et al., 2018). But the subicular network did not show such properties. These results suggest that novel components in both task demand and visual scene may be detected and processed primarily by the hippocampus, and the subiculum may not be functionally active until novelty subsides and the stimuli became familiar (Roy et al., 2017). Although the underlying mechanisms are unknown, our results indicate that the information processing between the hippocampus and subiculum is under dynamic control depending on task demands.

The lack of significant functional differences along the proximodistal axis in our study may be attributable simply to the inadequate sampling of neural activity especially in the distal area and the most proximal portion of the CA1. Another possibility is that the nature of the functional distinction between the proximal and distal portions of the region might be more complex in a goal-directed, complex memory task compared to random foraging situations (Henriksen et al., 2010) and simple behavioral paradigms (Cembrowski et al., 2018). For example, the perirhinal and postrhinal cortices, the upstream areas of the lateral and medial entorhinal cortices, respectively, also project directly to the CA1 and subiculum (Kosel et al., 1983; Naber et al., 1999; Witter, 2006). In our recent studies, I have shown that the functional distinctions at the perirhinal-postrhinal cortical level were less clear than at the entorhinal cortical level in the scene-dependent memory tasks although both perirhinal and postrhinal cortices play some significant roles in the tasks (Park et al., 2017; Yoo and Lee, 2017). It is possible

that there might be some dynamic interactions among the retrohippocampal cortices through the hippocampal formation when the rat is engaged in a goal-directed, complex memory task and a more sophisticated behavioral task is needed to dissociate these regions physiologically.

The schematic firing patterns of subicular cells in the current study might be contrasted with the diverse firing patterns of subicular neurons reported in prior studies (Brotons-Mas et al., 2017). One of the major differences is that I used a mnemonic task in the current study, whereas most prior studies recorded neural activity in a foraging paradigm using an open field. It is well known that goal-directed, structured information processing results in different firing properties in the hippocampal formation, compared to random foraging situations. For example, place cells in the hippocampus and subiculum tend to remap on a linear track as the rat passes the same locations from different directions to reach different goal locations (as opposed to the animal randomly foraging in an open field (McNaughton et al., 1983; Barnes et al., 1990; Geva-Sagiv et al., 2016). Also, changes in task demand such as rules and memory load alter the firing characteristics of hippocampal cells in goal-directed tasks (Markus et al., 1995; Hallock and Griffin, 2013). Although we did not record subicular cells in a foraging paradigm, it is possible that one might not be able to observe the schematic firing patterns reported in the current study if an animal randomly forages in an open field. This conjecture may be supported by the anatomical connections of the subiculum, showing independent and rich

connections with various regions other than the hippocampus (e.g., the amygdala, nucleus accumbens, retrosplenial cortex, prefrontal cortex, and retrohippocampal cortices) (Agster and Burwell, 2013; Cembrowski et al., 2018) that may play key roles in goal-directed memory tasks. Given a paucity of subicular recording studies using mnemonic tasks (Hampson and Deadwyler, 2003), our results may add valuable information to understanding the functional significance of subicular firing patterns in a memory task.

Bibliography

Agster KL, Burwell RD (2013) Hippocampal and subicular efferents and afferents of the perirhinal, postrhinal, and entorhinal cortices of the rat. Behav Brain Res 254:50-64.

Amaral DG, Dolorfo C, Alvarez-Royo P (1991) Organization of CA1 projections to the subiculum: a PHA-L analysis in the rat. Hippocampus 1:415-435.

Anderson MI, O'Mara SM (2003) Analysis of recordings of single-unit firing and population activity in the dorsal subiculum of unrestrained, freely moving rats. J Neurophysiol 90:655-665.

Anderson MI, Jeffery KJ (2003) Heterogeneous modulation of place cell firing by changes in context. J Neurosci 23:8827-8835.

Aronov D, Nevers R, Tank DW (2017) Mapping of a non-spatial dimension by the hippocampal-entorhinal circuit. Nature 543:719-722.

Barnes CA, McNaughton BL, Mizumori SJ, Leonard BW, Lin LH (1990) Comparison of spatial and temporal characteristics of neuronal activity in sequential stages of hippocampal processing. Prog Brain Res 83:287-300.

Behr J, Wozny C, Fidzinski P, Schmitz D (2009) Synaptic plasticity in the subiculum. Prog Neurobiol 89:334-342.

Behr J, Empson RM, Schmitz D, Gloveli T, Heinemann U (1996) Electrophysiological properties of rat subicular neurons in vitro. Neurosci Lett 220:41-44.

Bohm C, Peng Y, Maier N, Winterer J, Poulet JF, Geiger JR, Schmitz D (2015) Functional Diversity of Subicular Principal Cells during Hippocampal Ripples. J Neurosci 35:13608-13618.

Bos JJ, Vinck M, van Mourik-Donga LA, Jackson JC, Witter MP, Pennartz CMA (2017) Perirhinal firing patterns are sustained across large spatial segments of the task environment. Nat Commun 8:15602.

Brotons-Mas JR, Schaffelhofer S, Guger C, O'Mara SM, Sanchez-Vives MV (2017) Heterogeneous spatial representation by different subpopulations of neurons in the subiculum. Neuroscience 343:174-189.

Cembrowski MS, Phillips MG, DiLisio SF, Shields BC, Winnubst J, Chandrashekar J, Bas E, Spruston N (2018) Dissociable Structural and Functional Hippocampal Outputs via Distinct Subiculum Cell Classes. Cell 173:1280-1292 e1218.

Chang EH, Huerta PT (2012) Neurophysiological correlates of object recognition in the dorsal subiculum. Front Behav Neurosci 6:46.

Colgin LL, Moser EI, Moser MB (2008) Understanding memory through hippocampal remapping. Trends Neurosci 31:469-477.

Deadwyler SA, Hampson RE (2004) Differential but complementary mnemonic functions of the hippocampus and subiculum. Neuron 42:465-476.

Delcasso S, Huh N, Byeon JS, Lee J, Jung MW, Lee I (2014) Functional relationships between the hippocampus and dorsomedial striatum in learning a visual scene-based memory task in rats. J Neurosci 34:15534-15547.

Eichenbaum H (2000) A cortical-hippocampal system for declarative memory. Nat Rev Neurosci.

Ester M, Kriegel H-P, #246, Sander r, Xu X (1996) A density-based algorithm for discovering clusters a density-based algorithm for discovering clusters in large spatial databases with noise. In: Proceedings of the Second International Conference on Knowledge Discovery and Data Mining, pp 226-231. Portland, Oregon: AAAI Press.

Fidzinski P, Shor O, Behr J (2008) Target-cell-specific bidirectional synaptic plasticity at hippocampal output synapses. Eur J Neurosci 27:1111-1118.

Gaffan D (1994) Scene-Specific Memory for Objects: A Model of Episodic Memory Impairment in Monkeys with Fornix Transection. J Cog Neurosci.

Gaffan D, Harrison S (1989) Place memory and scene memory: effects of fornix transection in the monkey. Exp Brain Res 74:202-212.

Gauthier JL, Tank DW (2018) A Dedicated Population for Reward Coding in the Hippocampus. Neuron 99:179-193 e177.

Geva-Sagiv M, Romani S, Las L, Ulanovsky N (2016) Hippocampal global remapping for different sensory modalities in flying bats. Nat Neurosci 19:952-958.

Hallock HL, Griffin AL (2013) Dynamic coding of dorsal hippocampal neurons between tasks that differ in structure and memory demand. Hippocampus 23:169-186.

Hampson RE, Deadwyler SA (2003) Temporal firing characteristics and the strategic role of subicular neurons in short-term memory. Hippocampus 13:529-541.

Hampson RE, Hedberg T, Deadwyler SA (2000) Differential information processing by hippocampal and subicular neurons. Ann N Y Acad Sci 911:151-165.

Harris E, Witter MP, Weinstein G, Stewart M (2001) Intrinsic connectivity of the rat subiculum: I. Dendritic morphology and patterns of axonal arborization by pyramidal neurons. J Comp Neurol 435:490-505.

Harris KD, Csicsvari J, Hirase H, Dragoi G, Buzsaki G (2003) Organization of cell assemblies in the hippocampus. Nature 424:552-556.

Hassabis D, Kumaran D, Vann SD, Maguire EA (2007) Patients with hippocampal amnesia cannot imagine new experiences. Proc Natl Acad Sci U S A 104:1726-1731.

Hasselmo ME, Schnell E (1994) Laminar selectivity of the cholinergic suppression of synaptic transmission in rat hippocampal region CA1: computational modeling and brain slice physiology. J Neurosci 14:3898-3914.

Henriksen EJ, Colgin LL, Barnes CA, Witter MP, Moser MB, Moser EI (2010) Spatial representation along the proximodistal axis of CA1. Neuron 68:127-137.

Huxter J, Burgess N, O'Keefe J (2003) Independent rate and temporal coding in hippocampal pyramidal cells. Nature 425:828-832.

Jarsky T, Mady R, Kennedy B, Spruston N (2008) Distribution of bursting neurons in the CA1 region and the subiculum of the rat hippocampus. J Comp Neurol 506:535-547.

Kim JJ, Fanselow MS (1992) Modality-specific retrograde amnesia of fear. Science 256:675-677.

Kim S, Lee J, Lee I (2012a) The hippocampus is required for visually cued contextual response selection, but not for visual discrimination of contexts. Front Behav Neurosci 6:66.

Kim SM, Ganguli S, Frank LM (2012b) Spatial information outflow from the hippocampal circuit: distributed spatial coding and phase precession in the subiculum. J Neurosci 32:11539-11558.

Kim Y, Spruston N (2012) Target-specific output patterns are predicted by the distribution of regular-spiking and bursting pyramidal neurons in the subiculum. Hippocampus 22:693-706.

Knight R (1996) Contribution of human hippocampal region to novelty detection. Nature 383:256-259.

Kosel KC, Van Hoesen GW, Rosene DL (1983) A direct projection from the perirhinal cortex (area 35) to the subiculum in the rat. Brain Res 269:347-351.

Lee I, Kim J (2010) The shift from a response strategy to object-in-place strategy during learning is accompanied by a

matching shift in neural firing correlates in the hippocampus. Learn Mem 17:381-393.

Lee I, Yoganarasimha D, Rao G, Knierim JJ (2004) Comparison of population coherence of place cells in hippocampal subfields CA1 and CA3. Nature 430:456-459.

Lee KJ, Park SB, Lee I (2014) Elemental or contextual? It depends: individual difference in the hippocampal dependence of associative learning for a simple sensory stimulus. Front Behav Neurosci 8:217.

Leutgeb S, Leutgeb JK, Barnes CA, Moser EI, McNaughton BL, Moser MB (2005) Independent codes for spatial and episodic memory in hippocampal neuronal ensembles. Science 309:619-623.

Lever C, Burton S, Jeewajee A, O'Keefe J, Burgess N (2009) Boundary vector cells in the subiculum of the hippocampal formation. J Neurosci 29:9771-9777.

Maguire EA, Mullally SL (2013) The hippocampus: a manifesto for change. Journal of experimental psychology General 142:1180-1189.

Markus EJ, Qin YL, Leonard B, Skaggs WE, McNaughton BL, Barnes CA (1995) Interactions between location and task affect the spatial and directional firing of hippocampal neurons. J Neurosci 15:7079-7094.

Martin PD, Ono T (2000) Effects of reward anticipation, reward presentation, and spatial parameters on the firing of single neurons recorded in the subiculum and nucleus accumbens of freely moving rats. Behav Brain Res 116:23-38.

Matsumoto N, Kitanishi T, Mizuseki K (2019) The subiculum: Unique hippocampal hub and more. Neurosci Res 143:1-12.

Maurer AP, Cowen SL, Burke SN, Barnes CA, McNaughton BL (2006) Organization of hippocampal cell assemblies based on theta phase precession. Hippocampus 16:785-794.

McNaughton BL, Barnes CA, O'Keefe J (1983) The contributions of position, direction, and velocity to single unit activity in the hippocampus of freely-moving rats. Exp Brain Res 52:41-49.

Mullally SL, Hassabis D, Maguire EA (2012) Scene construction in amnesia: an FMRI study. J Neurosci 32:5646-5653.

Muller RU, Kubie JL (1987) The effects of changes in the environment on the spatial firing of hippocampal complex-spike cells. J Neurosci 7:1951-1968.

Naber PA, Witter MP (1998) Subicular efferents are organized mostly as parallel projections: a double-labeling, retrograde-tracing study in the rat. J Comp Neurol 393:284-297.

Naber PA, Witter MP, Lopez da Silva FH (1999) Perirhinal cortex input to the hippocampus in the rat: evidence for parallel pathways, both direct and indirect. A combined physiological and anatomical study. Eur J Neurosci 11:4119-4133.

Naber PA, Witter MP, Lopes da Silva FH (2001) Evidence for a direct projection from the postrhinal cortex to the subiculum in the rat. Hippocampus 11:105-117.

O'Keefe J, Dostrovsky J (1971) The hippocampus as a spatial map. Preliminary evidence from unit activity in the freely-moving rat. Brain Res 34:171-175.

O'Keefe J, Nadel L (1978) The Hippocampus as a Cognitive Map. Oxford Univ Press.

O'Keefe J, Recce ML (1993) Phase relationship between hippocampal place units and the EEG theta rhythm. Hippocampus 3:317-330.

O'Mara SM, Sanchez-Vives MV, Brotons-Mas JR, O'Hare E (2009) Roles for the subiculum in spatial information processing, memory, motivation and the temporal control of behaviour. Prog Neuropsychopharmacol Biol Psychiatry 33:782-790.

Olson JM, Tongprasearth K, Nitz DA (2017) Subiculum neurons map the current axis of travel. Nat Neurosci 20:170-172.

Park EH, Ahn JR, Lee I (2017) Interactions between stimulus and response types are more strongly represented in the entorhinal cortex than in its upstream regions in rats. Elife 6.

Potvin O, Dore FY, Goulet S (2007) Contributions of the dorsal hippocampus and the dorsal subiculum to processing of idiothetic information and spatial memory. Neurobiol Learn Mem 87:669-678.

Potvin O, Dore FY, Goulet S (2009) Lesions of the dorsal subiculum and the dorsal hippocampus impaired pattern separation in a task using distinct and overlapping visual stimuli. Neurobiol Learn Mem 91:287-297.

Potvin O, Lemay F, Dion M, Corado G, Dore FY, Goulet S (2010) Contribution of the dorsal subiculum to memory for temporal order and novelty detection using objects, odors, or spatial locations in the rat. Neurobiol Learn Mem 93:330-336.

Roy DS, Kitamura T, Okuyama T, Ogawa SK, Sun C, Obata Y, Yoshiki A, Tonegawa S (2017) Distinct Neural Circuits for the Formation and Retrieval of Episodic Memories. Cell 170:1000-1012 e1019.

Schmitzer-Torbert N, Jackson J, Henze D, Harris K, Redish AD (2005) Quantitative measures of cluster quality for use in extracellular recordings. Neuroscience 131:1-11.

Scoville WB, Milner B (1957) Loss of recent memory after bilateral hippocampal lesions. J Neurol Neurosurg Psychiatry 20:11-21.

Sharp PE (1997) Subicular cells generate similar spatial firing patterns in two geometrically and visually distinctive environments: comparison with hippocampal place cells. Behav Brain Res 85:71-92.

Sharp PE (2006) Subicular place cells generate the same "map" for different environments: comparison with hippocampal cells. Behav Brain Res 174:206-214.

Sharp PE, Green C (1994) Spatial correlates of firing patterns of single cells in the subiculum of the freely moving rat. J Neurosci 14:2339-2356.

Simonnet J, Brecht M (2019) Burst Firing and Spatial Coding in Subicular Principal Cells. J Neurosci 39:3651-3662.

Steward O (1976) Topographic organization of the projections from the entorhinal area to the hippocampal formation of the rat. J Comp Neurol 167:285-314.

Sun Y, Nguyen AQ, Nguyen JP, Le L, Saur D, Choi J, Callaway EM, Xu X (2014) Cell-type-specific circuit connectivity of hippocampal CA1 revealed through Cre-dependent rabies tracing. Cell Rep 7:269-280.

Sun Y, Jin S, Lin X, Chen L, Qiao X, Jiang L, Zhou P, Johnston KG, Golshani P, Nie Q, Holmes TC, Nitz DA, Xu X (2019) CA1-projecting subiculum neurons facilitate object-place learning. Nat Neurosci.

Treves A, Rolls ET (1994) Computational analysis of the role of the hippocampus in memory. Hippocampus 4:374-391.

Vinogradova OS (2001) Hippocampus as comparator: role of the two input and two output systems of the hippocampus in selection and registration of information. Hippocampus 11:578-598.

Witter MP (2006) Connections of the subiculum of the rat: topography in relation to columnar and laminar organization. Behav Brain Res 174:251-264.

Wouterlood FG, Saldana E, Witter MP (1990) Projection from the nucleus reuniens thalami to the hippocampal region: light and electron microscopic tracing study in the rat with the anterograde tracer Phaseolus vulgaris-leucoagglutinin. J Comp Neurol 296:179-203.

Yoo SW, Lee I (2017) Functional double dissociation within the entorhinal cortex for visual scene-dependent choice behavior. Elife 6.

국문 초록

시각장면기억 과제에서 해마이행부의 역할

이수민

어떠한 상황에 대해 판단하고 행동을 취해야 할 때, 우리는 대체로 주변 환경과 기억 속의 장면 정보를 활용한다. 해마와 해마이행부로 이루어진 해마체는 공간 기억과 일화 기억을 형성하는데 중요한 뇌 영역이므로, 해마체에서 시각 장면 정보가 어떻게 처리되는지 이해하는 것이 중요하다. 우리 연구실은 해마의 손상이 시각 장면 기억 과제의 수행 능력 저하를 일으킨다는 것을 보고한 바 있다. 또한 동일한 행동 과제에서 해마의 신경세포들이 장면 자극에 따라 발화율 변화를 보였다. 해마이행부의 손상 또한 과제수행력을 저해하였는데, 해마이행부의 신경 세포들이 장면 자극과 관련된 활성을 보이는지 검증한 연구 사례는 아직까지 없었다. 해마의 신경 세포가 세밀한 공간 표상을 보이는 반면, 해마이행부는 비교적 넓고 연속적인 공간 표상을 보이기 때문에 많은 선행 연구에서 해마이행부의 세포 활성 패턴을 이해하는 데에 어려움을 겪었다. 그러나 해마이행부는 해마의 정보를 가장 먼저 전달받는 영역이므로, 해마이행부의 세포 활성을 이해하는 것은 장면 정보 처리의 이해에 핵심적이다. 이 연구에서는 해마이행부의 신경 세포 활성을 이해하기 위해 2가지 분석 방법을 시도하였다. 첫 번째는 과제와 관련된 주요 시점들을 사용하여 세포 발화율 패턴을 조직하는 분석법이며, 두 번째는 지역적인 쎄타 진동에 대한 발화상을 발화율과 결합하여 활성 패턴을 분석하는 방법이다. 결과적으로, 장면 정보는 해마와 해마이행부가 비슷한 정도로

표상하였다. 그러나 해마가 좁은 공간을 세밀하게 표상하는데 비해, 해마이행부는 과제구조적인 표상을 가지거나 넓은 공간을 단위화하여 표상한다는 것을 밝혔다. 본 연구는 해마이행부의 복잡한 세포 활성 패턴을 해석하는 새로운 분석 패러다임을 제시하였으며, 시각 장면 기억 과제에서 신경 세포 활성에 대한 해마와 해마이행부 간의 차이점을 규명함으로써 단순한 정보 전달 매개체가 아닌 해마이행부 고유의 역할을 제안하였다.